Bioactive Materials 44 (2025) 205–219

Contents lists available at ScienceDirect

Bioactive Materials

journal homepage: www.keaipublishing.com/en/journals/bioactive-materials

Scaffolds functionalized with matrix metalloproteinase-responsive release of miRNA for synergistic magnetic hyperthermia and sensitizing chemotherapy of drug-tolerant breast cancer

Rui Sun [a,b], Man Wang [a,b], Tianjiao Zeng [a,b], Huajian Chen [a], Toru Yoshitomi [a], Masaki Takeguchi [c], Naoki Kawazoe [a], Yingnan Yang [d], Guoping Chen [a,b,*]

[a] Research Center for Macromolecules and Biomaterials, National Institute for Materials Science, Ibaraki, 305-0044, Japan
[b] Graduate School of Science and Technology, University of Tsukuba, Ibaraki, 305-8577, Japan
[c] Research Center for Energy and Environmental Materials, National Institute for Materials Science, Ibaraki, 305-0047, Japan
[d] Graduate School of Life and Environmental Science, University of Tsukuba, Ibaraki, 305-8572, Japan

ARTICLE INFO

Keywords:
Multifunctional scaffolds
Magnetic hyperthermia
Sensitizing chemotherapy
Tissue regeneration
Matrix metalloproteinase responsive
microRNA encapsulated liposomes

ABSTRACT

Combining hyperthermia and chemotherapy for maximum anticancer efficacy remains a challenge because drug-tolerant cancer cells often evade this synergistic treatment due to drug resistance and asynchronous drug release. In this study, multifunctional scaffolds were designed to efficiently treat drug-tolerant breast cancer by improving the sensitization of breast cancer cells and synchronizing anticancer drug release with magnetic hyperthermia. The scaffolds contained microRNA-encapsulated matrix metalloproteinase-cleavable liposomes, doxorubicin-encapsulated thermoresponsive liposomes and Fe_3O_4 nanoparticles. The scaffolds could release microRNA specifically to improve the sensitization of breast cancer cells to anticancer drugs. The scaffolds also showed excellent hyperthermia effects under alternating magnetic field irradiation. Moreover, doxorubicin release was synchronized with magnetic hyperthermia. *In vitro* and *in vivo* studies demonstrated that the scaffolds effectively reduced drug resistance and eliminated doxorubicin-tolerant MDA-MB-231 cells through the synergistic effect of magnetic hyperthermia and sensitizing chemotherapy. Additionally, the scaffolds could support the proliferation and adipogenic differentiation of stem cells for adipose tissue regeneration after killing cancer cells at a late therapeutic stage. These composite scaffolds offer an innovative strategy for treating breast cancer, with synergistic anticancer effects and regenerative functions.

1. Introduction

Breast cancer accounts for the highest number of fatalities among women diagnosed with cancer [1]. Currently, surgery, chemotherapy and radiotherapy are extensively utilized in the clinical treatment of breast cancer [2–4]. However, these conventional methods have inherent limitations that often lead to unexpected treatment outcomes [5–7]. In recent years, hyperthermia has been developed as a promising approach to treat breast cancer [8,9]. Various nanomaterials have been reported for cancer hyperthermia, including Au nanoparticles (NPs), black phosphorus nanosheets and Fe_3O_4 NPs [10–18]. Fe_3O_4 NPs can convert magnetic energy into heat when irradiated by an alternating magnetic field (AMF), known as magnetic hyperthermia [19,20]. Due to their low cytotoxicity, deep tissue penetration and FDA approval, Fe_3O_4 NPs have been extensively studied as heat conversion agents for magnetic hyperthermia [21–23]. In general, NPs are delivered systemically by intravenous injection, but they are easily and rapidly cleared by the body's metabolic system, which leads to low accumulation and retention of NPs in cancer tissues [24,25]. To overcome the drawbacks of intravenous injection, scaffolds have been used as effective platforms for the local delivery of NPs [26–33]. Scaffolds incorporating Fe_3O_4 NPs can constrain NPs at cancer sites and be irradiated by AMF for magnetic hyperthermia.

However, a single therapeutic strategy cannot eliminate all cancer cells due to the heterogeneity of cancer tissue and resistance to monotherapy [34,35]. To solve monotherapy problems, combinations of

Peer review under responsibility of KeAi Communications Co., Ltd.
* Corresponding author. Research Center for Macromolecules and Biomaterials, National Institute for Materials Science, Ibaraki, 305-0044, Japan.
E-mail address: Guoping.CHEN@nims.go.jp (G. Chen).

https://doi.org/10.1016/j.bioactmat.2024.10.011
Received 24 July 2024; Received in revised form 19 September 2024; Accepted 11 October 2024
Available online 19 October 2024

different therapeutic strategies, such as hyperthermia and chemotherapy, have been studied to achieve collective advantages for increased anticancer effects [36–38]. However, simply combining hyperthermia and chemotherapy cannot maximize the synergistic therapeutic effect because the release of anticancer drugs is uncontrollable and independent of magnetic hyperthermia. Synchronizing magnetic hyperthermia and chemotherapy by controlling the release of anticancer drugs from the hyperthermal microenvironment should be considered. To address this problem, thermosensitive liposomes can be utilized as a means of delivering drugs in response to the hyperthermal microenvironment. Liposomes prepared from 1,2-dipalmitoyl-sn-glycero-3-phosphocholine (DPPC) exhibit thermosensitive release properties at temperatures greater than 41 °C, good biocompatibility and high drug payloads [39,40]. Thus, scaffolds incorporating thermosensitive liposomes can be endowed with temperature-responsive release properties, allowing for controlled drug release through magnetic hyperthermia stimulation to synchronize the therapeutic effects of magnetic hyperthermia and chemotherapy.

Another challenge is the intrinsic or acquired drug resistance of cancer cells, which remains one of the main obstacles in chemotherapy [41–43]. Increasing the sensitization of cancer cells is necessary to reduce their drug resistance. MicroRNAs (miRNAs) are good candidates for overcoming drug resistance because they can affect the expression of different genes and are involved in multiple mechanisms associated with cancer cell activities, such as apoptosis, proliferation and invasion. miR-200c, a member of the miRNA family, plays a crucial role as a drug resistance gene suppressor in various types of cancers, including breast cancer, where its expression is often downregulated [44,45]. The miR-200c can influence the expression of drug transporters, such as multidrug resistance 1 (MDR1, P-glycoprotein), which are responsible for the efflux of chemotherapeutic agents from cancer cells [46]. High MDR1 levels can result in reduced intracellular drug concentrations and decreased drug efficacy. An increase in miR-200c decreases the expression levels of these transport proteins, leading to reduced drug resistance. Therefore, controlling the precise delivery of miRNA-encapsulated liposomes to cancer cells is crucial for maximizing the drug resistance-associated gene inhibitory effect. To achieve precise intratumoral delivery, the utilization of specific stimuli in the tumor microenvironment, such as pH, hypoxia and proteases, can be considered [47,48]. Matrix metalloproteinase-7 (MMP-7), which is overexpressed by various cancer cells, can act as a triggering enzyme for the cleavage of specific peptide sequences [49–53]. Therefore, miRNAs can be encapsulated in liposomes, which are linked to the scaffolds through an MMP-7-cleavable peptide crosslinker, to achieve precise delivery of miRNAs to drug-resistant cancer cells.

After eliminating breast cancer cells, the breast tissue defects caused by surgical resection require reconstruction to restore breast tissue functions to increase patient quality of life. Biodegradable polymer scaffolds with porous structures have been widely employed for tissue regeneration. Notably, gelatin and polyglutamic acid scaffolds have garnered significant interest because of their biomimetic composition and excellent biocompatibility [54,55]. Consequently, composite

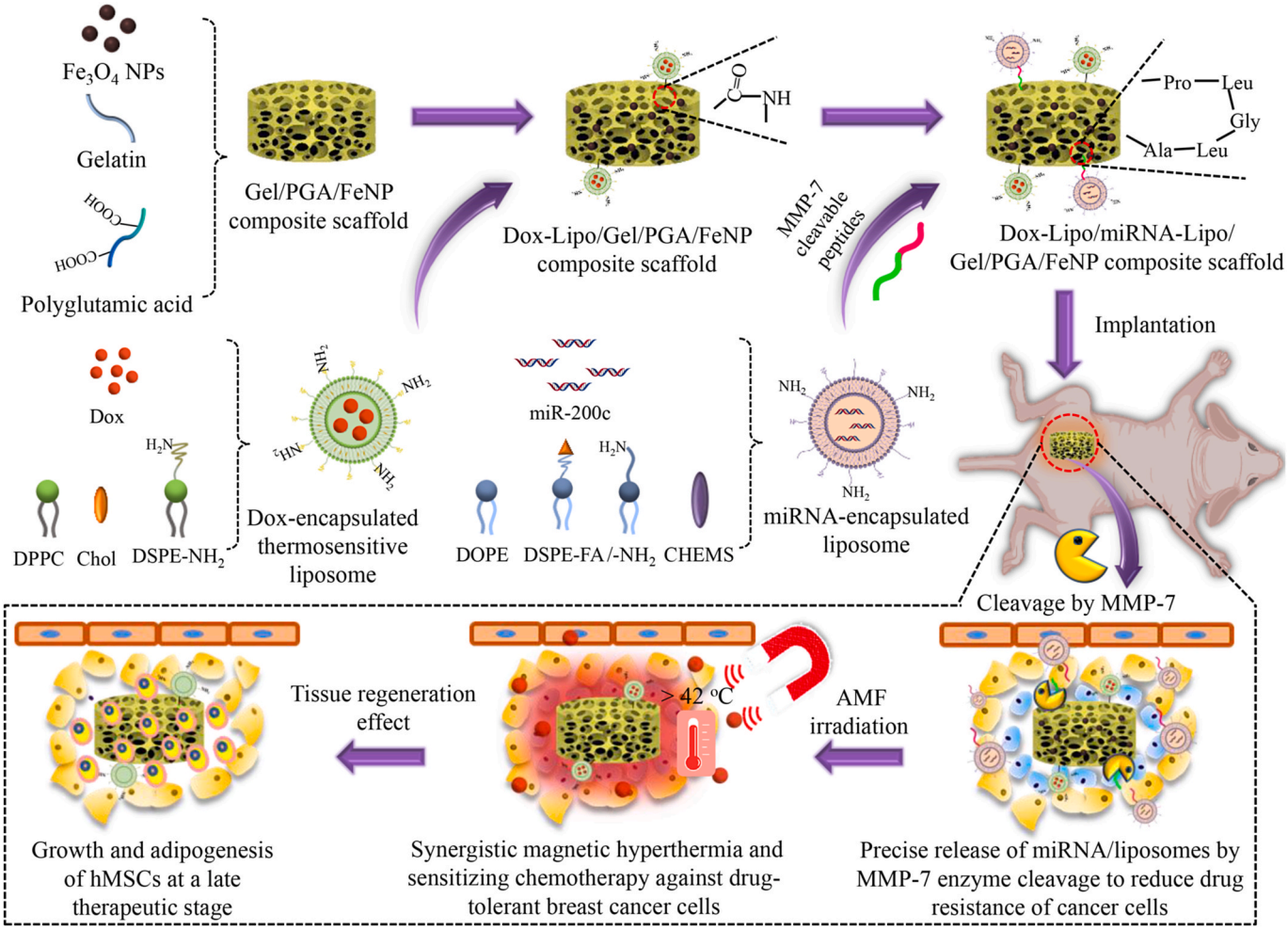

Scheme 1. Schematic diagram of preparation of multifunctional composite scaffolds and their applications for synergistic magnetic hyperthermia and sensitizing chemotherapy of drug-tolerant breast cancer and regeneration of breast tissue.

scaffolds with dual functions (anticancer effects and tissue regeneration capabilities) are needed to facilitate effective breast cancer treatment.

Based on the above considerations, miRNA-encapsulated matrix metalloproteinase-cleavable liposomes (miRNA-Lipo) and doxorubicin (Dox)-encapsulated thermosensitive liposomes (Dox-Lipo) were hybridized with Fe_3O_4 NPs (FeNP), gelatin (Gel) and polyglutamic acid (PGA) using preprepared ice microparticles as a porogen material to prepare multifunctional scaffolds (Dox-Lipo/miRNA-Lipo/Gel/PGA/FeNP) for a combination of magnetic hyperthermia, sensitizing chemotherapy and tissue regeneration (Scheme 1). Ice microparticles served as the porogen to dominate the pore structure of the composite scaffolds. PGA was utilized to subjoin the carboxyl groups in the composite scaffolds for immobilization of Dox-Lipo. The MMP-7-cleavable peptide was used as a crosslinker between the composite scaffolds and miRNA-Lipo. The magnetic thermal performance and temperature-controlled Dox release properties of the composite scaffolds were investigated under AMF irradiation. The specific MMP-7-responsive release and endocytosis of miRNA-Lipo were investigated in Dox-tolerant breast cancer cells. The synergistic anticancer effect of the composite scaffolds was studied in *in vitro* cell culture and *in vivo* animal experiments under AMF irradiation. Furthermore, after miRNA-Lipo and Dox were completely released, human bone marrow-derived mesenchymal stem cells (hMSCs) were cultured in the composite scaffolds to evaluate their ability to promote the growth and adipogenesis of hMSCs. The composite scaffolds were also evaluated for their *in vivo* tissue regeneration potential.

2. Materials and methods

2.1. Preparation of Fe_3O_4 NPs

Fe_3O_4 NPs were prepared using a previously reported method [54]. Briefly, diethylene glycol (DEG) and N-methyldiethanolamine (NMDEA) were mixed (1:1, v/v). A total of 270 mg of $FeCl_3{\bullet}6H_2O$ and 100 mg of $FeCl_2{\bullet}4H_2O$ were dissolved in 20 mL of the DEG/NMDEA mixture solvent under a N_2 atmosphere. Then, 160 mg of NaOH in a mixture solvent of DEG and NMDEA was added to the solution of iron salts and stirred for 3 h. Subsequently, the solution was heated to 220 °C for 1 h and stirred at 500 rpm for 12 h in a N_2 atmosphere. After that, black sediments were collected and washed with an ethanol/ethyl acetate mixture (1:1, v/v) to obtain bare Fe_3O_4 NPs. The bare Fe_3O_4 NPs were modified with citrate by adding 132.5 mg of sodium citrate dihydrate to the NPs aqueous solution and reacting at 60 °C for 24 h. Citrate ions can form coordination complexes with metal ions on the Fe_3O_4 NP surface. This complexation can further stabilize the dispersion by altering the surface charge of the nanoparticles and preventing them from agglomerating. The citrate-modified Fe_3O_4 NPs were centrifuged at high speed for 15 min (12,000 rpm), washed three times with pure water and dried. Transmission electron microscopy (JEOL, JEM-ARM200F) and dynamic light scattering (DLS, Beckman Coulter) were used to characterize the structure and hydrodynamic size of the citrate-modified Fe_3O_4 NPs. Citrate-modified Fe_3O_4 NPs were used for all the following experiments. The normalized field-dependent magnetization (M − H) curve of the NPs was measured on a Physical Property Measurement System (PPMS, PPMS DynaCool, CA, USA). Hysteresis analysis was conducted in a field region of ±10,000 Oe at 300 K.

2.2. Preparation of Dox-encapsulated thermosensitive liposomes

Cholesterol (Chol), 1,2-distearoyl-sn-glycero-3-phosphoethanolamine-N-[amino-(polyethylene glycol)-2000] (ammonium salt) (DSPE) and DPPC were used for the preparation of Dox-encapsulated DPPC/Chol/DSPE liposomes (Dox-Lipo) by a thin film hydration method [56]. Briefly, 0.60 mL of DPPC (5 mg/mL), 0.08 mL of cholesterol (5 mg/mL) and 0.32 mL of DSPE (5 mg/mL) (molar ratio of DPPC:Chol:DSPE = 7:2:1) in a chloroform/methanol mixture solvent were added to a round bottom flask. The flask was connected to a rotary evaporator to evaporate the chloroform/methanol mixture under vacuum, and a thin film formed. Then, 1 mL of Dox in PBS solution (1 mg/mL) was added to the flask for hydration, and the flask was sonicated at 45 °C for 0.5 h. After sonication, the solution was extruded at 45 °C through a polycarbonate membrane (200 nm aperture). The extrusion solution was centrifuged at 20,000 rpm for 15 min, and the reddish sediments were washed, resuspended in 1 mL of PBS, and stored below 4 °C. TEM and DLS were used to characterize the structure and hydrodynamic size of the liposomes before and after Dox loading. The amount of Dox in the liposomes was measured by destroying the liposomes with a chloroform/methanol mixture and analyzing them with a fluorescence spectrophotometer. The encapsulation efficiency was calculated by dividing the encapsulated amount of Dox by the initial feeding amount of Dox.

2.3. Preparation of miRNA-liposomes and MMP-7-cleavable peptide modifications

1,2-Dioleoyl-sn-glycero-3-phosphoethanolamine (DOPE), 1,2-distearoyl-sn- glycero-3-phosphoethanolamine-N-[amino-(polyethyleneglycol)-2000] (ammonium salt) (DSPE), 1,2-distearoyl-sn-glycero-3-phosphoethanolamine-N-[amino-(polyethyleneglycol)-2000-folic acid] (DSPE-FA) and cholesteryl hemisuccinate (CHEMS) were used for the preparation of miRNA-encapsulated DOPE/CHEMS/DSPE liposomes (miRNA-Lipo) by the thin film hydration method. The miR-200c sequence (5′-3′) was UAAUACUGCCGGGUAAUGAUGGA. Briefly, 0.56 mL of DOPE (5 mg/mL), 0.23 mL of CHEMS (5 mg/mL), 0.17 mL of DSPE-FA (5 mg/mL) and 0.04 mL of DSPE (5 mg/mL) (molar ratio of DOPE:CHEMS:DSPE-FA:DSPE = 5.8:3.7:0.4:0.1) in a chloroform/methanol mixture solvent were added to a round bottom flask, and the flask was connected to a rotary evaporator to evaporate the chloroform/methanol mixture under vacuum. The formed lipid thin film was hydrated to prepare miRNA/DOPE/CHEMS/DSPE liposomes. 1 mL of miRNA solution (DEPC water, 20 μM) was added to the flask for hydration, and the flask was sonicated in an ice bath for 5 min. After sonication, the solution was extruded at room temperature through a polycarbonate membrane (200-nm aperture). The extrusion solution was centrifuged at 20,000 rpm for 15 min, and the sediments were washed and resuspended in 1 mL of PBS for further use. TEM and DLS were used to characterize the structure and hydrodynamic size of the liposomes before and after miRNA loading. The amount of miRNA (labeled with Cy5) in the liposomes was measured by destroying the liposomes with a chloroform/methanol mixture and analyzing them with a fluorescence spectrophotometer. The encapsulation efficiency was calculated by dividing the encapsulated amount of miRNA by the initial feeding amount of miRNA.

The MMP-7-cleavable peptide-modified miRNA-Lipo was prepared by conjugating the peptide to the miRNA-Lipo. The peptide sequence was N_3-GGGPLGLAGGG-CO-NHS [50,51]. Briefly, 16.2 μg of peptide was added to 1 mL of the miRNA-Lipo suspension prepared as described above and reacted at 4 °C for 6 h. Then, the reaction mixture was centrifuged at 20,000 rpm for 15 min to obtain peptide-modified miRNA-Lipo. The prepared liposomes were further washed and resuspended in 1 mL of PBS and stored below 4 °C for further use.

2.4. Preparation of composite scaffolds of Fe_3O_4 NPs, Gel and PGA

The lyophilizing Fe_3O_4 NPs, Gel and PGA were hybridized to synthesize their composite scaffolds (Fig. S1). Ice microparticles as porogen materials were used to control the pore structure. We first prepared uniform ice microparticles by spraying water into liquid nitrogen and sieving the pre-ice microparticles (Fig. S1A). Then, we mixed the Fe_3O_4 NPs with gelatin and PGA (polyglycolic acid) solutions in acetic acid (Fig. S1B). Both the ice microparticles and the mixtures were then placed at −5 °C for equilibration. The acetic acid solvent ensured that the mixed solution remained in a liquid state at −5 °C and prevented the

subsequent addition of ice microparticles from melting. After balancing the temperature, we mixed the ice microparticles with the mixtures and transferred the mixtures to a mold (Fig. S1C). The mold was frozen, and during the freeze–drying process, uniformly sized pores formed. Moreover, during the freezing process, new ice crystals grew on the surface of the ice microparticles, forming interconnected pores. This series of operations generated the Gel/PGA/FeNP scaffold. The details are as follows. First, pure water was sprayed into a box filled with liquid nitrogen to prepare pre-ice microparticles. Then, the pre-ice microparticles were sieved in a −20 °C chamber with two sieves to obtain uniform microparticles with diameters of 250–355 μm. After that, 132.0 mg (8 % (wt/v)) of Gel and 13.2 mg (0.8 % (wt/v)) of PGA were dissolved in 1.65 mL of 70 % acetic acid solution to obtain a Gel/PGA mixture. 220 mg of Fe_3O_4 NPs was resuspended in 1.65 mL of pure water. A total of 1.65 mL of the Fe_3O_4 NP mixture was added to 1.65 mL of the Gel/PGA mixture and vortexed to obtain a Gel/PGA/FeNP mixture (3.3 mL). The Gel/PGA/FeNP mixture and ice microparticles were placed at −5 °C in advance to balance the temperature. Then, 7.7 g of ice microparticles was added to 3.3 mL of the Gel/PGA/FeNP mixture (7:3 (wt/v)) in the −5 °C chamber. The as-prepared mixture of ice microparticles and Gel/PGA/FeNP solution was transferred into a silicone mold (length 60 mm × width 60 mm × height 6 mm), and the whole constructs were frozen at −20 °C, lyophilized for 3 days, and cross-linked with ethanol/water mixed solutions (95/5, 90/10 and 85/5 (v/v)) containing 4-morpholineethanesulfonic acid (0.1 % (wt/v)), 1-ethyl-3-(3-dimethylaminopropyl) carbodiimide (EDC, 50.0 mM) and N-hydroxysuccinimide (NHS, 20.0 mM). The resulting Gel/PGA/FeNP scaffolds were subsequently washed and lyophilized for further use. Gel/PGA scaffolds were also prepared through the same procedure without the addition of Fe_3O_4 NPs. Scanning electron microscopy (SEM, JSM-6400Fs) was used for characterization of the pore structures. For SEM observation, samples were also generated by punching them into discs (Φ6 mm × H2 mm). The punching process to generate scaffold discs did not significantly affect the microscopic morphology or the mechanical, magnetic thermal or drug release properties of the scaffold itself.

2.5. Preparation of composite scaffolds coloaded with Dox-Lipo and miRNA-Lipo

Dox-Lipo and miRNA-Lipo were coupled onto Gel/PGA/FeNP composite scaffolds through amidation and click reactions, respectively, to fabricate Dox-Lipo/miRNA-Lipo/Gel/PGA/FeNP composite scaffolds. First, the Gel/PGA/FeNP scaffolds were punched into discs (Φ6 mm × H2 mm), and the scaffold discs were immersed in EDC/NHS solution at room temperature overnight to activate the carboxyl groups. Then, 57 μL of N-[(1R,8S,9s)-bicyclo[6.1.0]non-4-yn-9-ylmethyloxycarbonyl]-1,8-diamino-3,6-dio-xaoctane (BCN-NH_2, 0.23 mg/mL) solution was added to the discs and allowed to react at room temperature for 12 h. The unbound BCN-NH_2 was removed by washing with PBS. After that, the discs were immersed in EDC/NHS solution for 12 h, and 57 μL of Dox-Lipo solution (Dox at 0.5 mg/mL) was added to the discs and allowed to react at room temperature for another 12 h. After the unbound Dox-Lipo was removed, the obtained Dox-Lipo/Gel/PGA/FeNP composite scaffolds were immersed in 0.1 M glycine solution overnight for blocking. Then, 57 μL of miRNA-Lipo solution (miRNA at 12.6 μM) was added to the discs and reacted at 4 °C for 12 h. The prepared Dox-Lipo/miRNA-Lipo/Gel/PGA/FeNP composite scaffolds were then washed and stored below 4 °C for further use. The Dox-Lipo/miRNA-Lipo/Gel/PGA scaffolds were prepared by the same procedure. The structures of the composite scaffolds were analyzed by SEM. The amounts of Dox and miRNA (labeled with Cy5) incorporated into the Dox-Lipo/miRNA-Lipo/Gel/PGA/FeNP composite scaffolds were measured by destroying the liposomes in the scaffolds with a chloroform/methanol mixture and analyzing them with a fluorescence spectrophotometer. The loading efficiencies of Dox-Lipo and miRNA-Lipo were calculated by dividing the loaded amount of Dox or miRNA in the composite scaffolds by the initial feeding amount of Dox or miRNA.

2.6. Biostability of the composite scaffolds

The biostability of the composite scaffolds was evaluated by immersing them in PBS without or with collagenase. The Gel/PGA and Dox-Lipo/miRNA-Lipo/Gel/PGA/FeNP composite scaffolds were lyophilized, preweighed, and soaked in PBS without or with 50 μg/mL of collagenase at 37 °C under shaking. At the designated timepoints, the Gel/PGA and Dox-Lipo/miRNA-Lipo/Gel/PGA/FeNP composite scaffolds were removed, washed with pure water six times, lyophilized and weighed. The remaining weight was calculated by dividing the residual weight of the scaffolds by the original weight of the scaffolds.

2.7. Magnetic thermal conversion performance of the composite scaffolds

The magnetic thermal performance of the scaffolds was investigated during AMF irradiation. The Gel/PGA, Gel/PGA/FeNP, Dox-Lipo/miRNA-Lipo/Gel/PGA, Dox-Lipo/Gel/PGA/FeNP, and Dox-Lipo/miRNA-Lipo/Gel/PGA/FeNP composite scaffold discs were placed inside silicone frames (Φ6 mm × H2 mm), and 57 μL of pure water was added to each disc. The hydrated discs were placed in Double H CoilSets for AMF (373.6 kHz, 100 Gauss) and irradiated for 10 min (D5 Series, Spain), which was based on the previously optimized AMF irradiation conditions [29]. The temperature changes of the scaffold discs were recorded when they were irradiated by AMF using an IR1 thermal image system (nB nanoScale Biomagnetics, Spain). The normalized field-dependent magnetization (M − H) curve of the NPs in the Dox-Lipo/miRNA-Lipo/Gel/PGA/FeNP composite scaffolds was measured under the same conditions as that of the free NPs.

2.8. Dox release from composite scaffolds under AMF irradiation

The temperature-dependent release of Dox from the composite scaffolds was evaluated by periodic AMF irradiation. Each disc was immersed in a well of a 24-well plate with 1 mL of PBS per well and shaken at 37 °C. After 1 day of incubation, the scaffold discs were placed in a 0.5 mL sterile tube covered with a Styrofoam box, and the whole construct was then irradiated with AMF (373.6 kHz, 100 Gauss) for 10 min. After AMF irradiation, the discs were returned to the wells and incubated at 37 °C. AMF irradiation was conducted every 24 h after incubation. At time points before and after each period of AMF irradiation, 100 μL of PBS was removed from each well for measurement, and then 100 μL of fresh PBS was added to each well. The amount of Dox released from the discs was analyzed with a fluorescence spectrophotometer, and the cumulative amount of Dox was calculated. The Dox release properties of the composite scaffolds incubated at 37 °C were also assessed using the same procedure but not by irradiation with AMF.

2.9. miRNA-Lipo cleaved from composite scaffolds by MMP-7

The release of the enzyme-cleaved miRNA-Lipo from the composite scaffolds was studied using the Dox-Lipo/miRNA-Lipo/Gel/PGA/FeNP composite scaffold under MMP-7 treatment. Previous studies have shown that MMP-7 concentrations across various types of cancer range from 0.6 to 143 μg/mL, with an average tissue concentration of 20.9 μg/mL [52,57]. Additionally, some studies have confirmed that the concentration of MMP-7 in the supernatant of tumor cells cultured in medium can reach 2.0 μg/mL, which can effectively cleave the -PLGLA-peptide [51]. Based on these findings, we used this concentration in similar experimental setups. The composite scaffolds (Φ6 mm × H2 mm) were immersed in 24-well plates with 1 mL of MMP-7 solution (2 μg/mL) and shaken at 37 °C. After 2 or 12 h of incubation, the composite scaffold discs were removed, a chloroform/methanol mixture was added to each well, and the mixture was subsequently measured with a fluorescence spectrophotometer. The cleavage efficiency of the

miRNA-Lipo was calculated by dividing the cleaved amount of miRNA in the liposomes by the initial amount of miRNA in the scaffolds.

2.10. Cellular uptake of miRNA-Lipo from composite scaffolds

The cellular uptake of miRNA-Lipo cleaved from the composite scaffolds was observed by culturing Dox-tolerant cancer cells with Dox-Lipo/miRNA-Lipo/Gel/PGA/FeNP composite scaffolds. The resistance of MDA-MB-231 cells to Dox was established using a commonly reported method of exposing cells to a continuous concentration of the drug over multiple generations [58,59]. Specifically, parental cells were exposed to medium supplemented with a constant concentration of Dox (50 nM) for 15 passages. After this treatment, the half-maximal inhibitory concentration (IC_{50}) of the resistant cells was 3.2 μM, which was approximately 3.6 times greater than the IC_{50} of the initial passage (P0), which was 0.9 μM (Fig. S2). Stable Dox-resistant MDA-MB-231 cells were then cultured in the presence of Dox (50 nM) to maintain the drug resistance phenotype and were used in this study. A total of 2×10^4 cells were seeded in glass-bottom dishes (Φ14 mm) and cultured for 3 days. The composite scaffold discs (Φ6 mm × H2 mm) were immersed in glass-bottom dishes supplemented with 2 μg/mL of MMP-7. After 1 day of incubation, the scaffold discs were removed, and the cells were washed with PBS. The cells were subsequently stained with LysoTracker™ Green DND-26 and Hoechst 33258 to image lysosomes and nuclei, respectively. After staining, the cells were washed with PBS and observed by confocal laser scanning microscopy.

2.11. In vitro synergistic anticancer effects of the composite scaffolds

In vitro synergistic therapy of the composite scaffolds was evaluated by performing periodic AMF irradiation of the scaffold discs seeded with Dox-tolerant MDA-MB-231 cells. Dox-tolerant MDA-MB-231 cells were subcultured and harvested by trypsinization. The collected cells were resuspended in DMEM (3.6×10^6 cells/mL). 57 μL of resuspended Dox-tolerant MDA-MB-231 cell mixture was added to one side of the scaffold discs (Φ6 mm × H2 mm), and the cells/scaffold discs were incubated in a humidified incubator for 6 h. Then, 57 μL of resuspended cells was added to the other side of the discs and incubated for another 6 h (4.1×10^5 cells on each scaffold disc). Moreover, the resuspended cells were seeded in 24-well plates and cultured for 6 h. Then, the cells/scaffold discs were placed in Transwell inserts and cocultured in 24-well plates. Each well, including the insert, contained 1 mL of DMEM with 2 μg/mL of MMP-7. The Transwell insert had a PET membrane with 8 μm pores, making it possible to diffuse the released miRNA-Lipo and Dox. After 24 h of coculture, the cell/scaffold discs on the inserts of the Transwell plates were removed and placed in a 0.5 mL sterile tube covered with a Styrofoam box for 10 min of AMF irradiation (373.6 kHz, 100 Gauss). After AMF irradiation, the cell/scaffold discs were returned to the Transwell inserts immediately and incubated for another 24 h. AMF irradiation was conducted every 24 h after coculture. At time points before and after each period of AMF irradiation, the scaffold discs were stained with a live/dead staining kit and observed by fluorescence microscopy. The viability of Dox-tolerant MDA-MB-231 cells in the scaffold discs and bottom wells of 24-well plates was analyzed by WST-1 assay, which is a colorimetric assay used to assess cell viability and proliferation.

2.12. In vivo synergistic anticancer effects of the composite scaffolds

Animal experiments were conducted with approval from the Ethical Committee of Animal Experiments of NIMS (accreditation No: 76-2023-12) and according to the Committee Guidelines. Dox-tolerant MDA-MB-231 cells were seeded onto scaffold discs (Φ6 mm × H2 mm) of Gel/PGA, Gel/PGA/FeNP, Dox-Lipo/miRNA-Lipo/Gel/PGA, Dox-Lipo/Gel/PGA/FeNP and Dox-Lipo/miRNA-Lipo/Gel/PGA/FeNP. To simulate the residual breast cancer cells surrounding the scaffolds, a donut-shaped porous scaffold ring seeded with Dox-tolerant MDA-MB-231 cells was applied to surround the scaffold discs. The donut-shaped porous scaffold rings were prepared by punching the Gel/PGA scaffolds into rings (inner diameter: 6 mm, outer diameter: 10 mm and thickness: 2 mm). A 100 μL resuspension of Dox-tolerant MDA-MB-231 cells (3.6×10^6 cells/mL) was dripped onto each side of the donut-shaped porous scaffold rings and incubated in a humidified incubator for 6 h after two side-seeding (7.2×10^5 cells on each scaffold ring), which ensured that the number of tumor cells and the composition across all the experimental groups were consistent. After incubation, the cells/scaffold discs were set into the inner space of the cells/donut-shaped porous scaffold rings and were implanted together in the backs of the BALB/c nude mice. One day after implantation, the implantation sites were irradiated with AMF for 10 min (373.6 kHz, 100 Gauss). During AMF irradiation, thermal images and the temperatures of the mice were recorded using an IR camera. Periodic AMF irradiation was performed every 1 or 2 days. Before and after each period of AMF irradiation, the viability of Dox-tolerant MDA-MB-231 cells in the scaffold discs and surrounding scaffold rings was evaluated using an *in vivo* visualization system (IVIS, PerkinElmer) with a previously reported method [54]. Cancer cell growth was monitored in bioluminescence images. The survival rate of the mice was recorded at 28 days. Each scaffold group was implanted in four mice (n = 4).

2.13. Biodistribution and histology analysis

As described above for *in vivo* anticancer treatment, the mice were implanted with the cell/composite scaffold discs and cell/scaffold rings. On Days 1 and 14 after five rounds of AMF irradiation, various organs, such as the heart, liver, spleen, lung, kidney, stomach and blood, were removed from the mice, wet-weighed, and digested in digestion solution (HNO_3:H_2O_2 ratio of 2:1 by volume). The contents of Fe in each tissue sample were determined by ICP–OES. Moreover, on Days 1 and 14 after the therapeutic experiments, the mice were sacrificed, and their major organs (heart, liver, spleen, lung and kidney) were harvested, fixed in 4 % paraformaldehyde solution, dehydrated, and embedded in paraffin. A series of 7 μm thick slices were subsequently prepared and stained with hematoxylin–eosin (H&E). The histology and morphology of the organs were observed using an optical microscope.

2.14. Proliferation and adipogenesis of stem cells in composite scaffolds after drug release

The influence of the composite scaffolds after full drug release on the viability and proliferation of hMSCs was investigated. Before cell seeding, the Dox-Lipo/miRNA-Lipo/Gel/PGA/FeNP scaffold discs were immersed in 1 mL of MMP-7 enzyme solution and irradiated with AMF (373.6 kHz, 100 Gauss) until no released miRNA-Lipo or Dox was detected from the scaffold discs. Then, the scaffold discs were washed 6 times with PBS and seeded with hMSCs. The hMSCs were subcultured, harvested, and resuspended in culture medium (3.6×10^6 cells/mL). The resuspended hMSCs were seeded on each side of the scaffold discs (57 μL per side) and incubated in a humidified incubator for 6 h after each seeding. After seeding, the hMSC/scaffold constructs were placed in a flask and incubated under shaking. After 1 day of incubation, the cell viability and distribution in the scaffold discs were investigated by live/dead staining, nuclear staining and SEM observation. After culturing for 1, 3, 5 and 7 days, the DNA contents of the hMSCs in the scaffold discs were measured using a previously reported method [54].

For the adipogenesis of hMSCs in the composite scaffolds, after 1 day of incubation, the cells/scaffold discs were divided into two groups. One group of the cells/scaffold discs was maintained in culture medium (basal), and the other group of cells/scaffold discs was cultured in adipogenesis-inducing medium containing adipogenesis-inducing factors. Basal and adipogenesis-inducing medium were prepared using a previously reported method [15]. After 21 days of culture, the adipogenesis of hMSCs in the scaffold discs was analyzed by lipid droplet

staining and real-time PCR using a previously reported method [15].

2.15. In vivo tissue regeneration

As described above for *in vivo* anticancer treatment, the mice were implanted with cells/composite scaffold discs and cell/scaffold rings. On Days 14 and 28 after the therapeutic experiments, the mice were sacrificed, and the implanted scaffold constructs were retrieved for observation by optical microscopy. The retrieved scaffold constructs were subsequently fixed in 4 % paraformaldehyde solution for 24 h at room temperature. The fixed cell/scaffold constructs were dehydrated, embedded in paraffin, and sliced with a microtome to obtain cross-sections at a thickness of 7 μm. The slices were stained with H&E and observed by optical microscopy.

2.16. Statistical analysis

The *in vitro* and *in vivo* quantitative experiments were conducted using triplicate and quadruplicate samples, respectively. The data are expressed as the means ± standard deviations. Two-tailed t tests were used to determine the significance of differences between two groups. One-way ANOVA with Tukey's post hoc test in Origin Pro software (8.0)

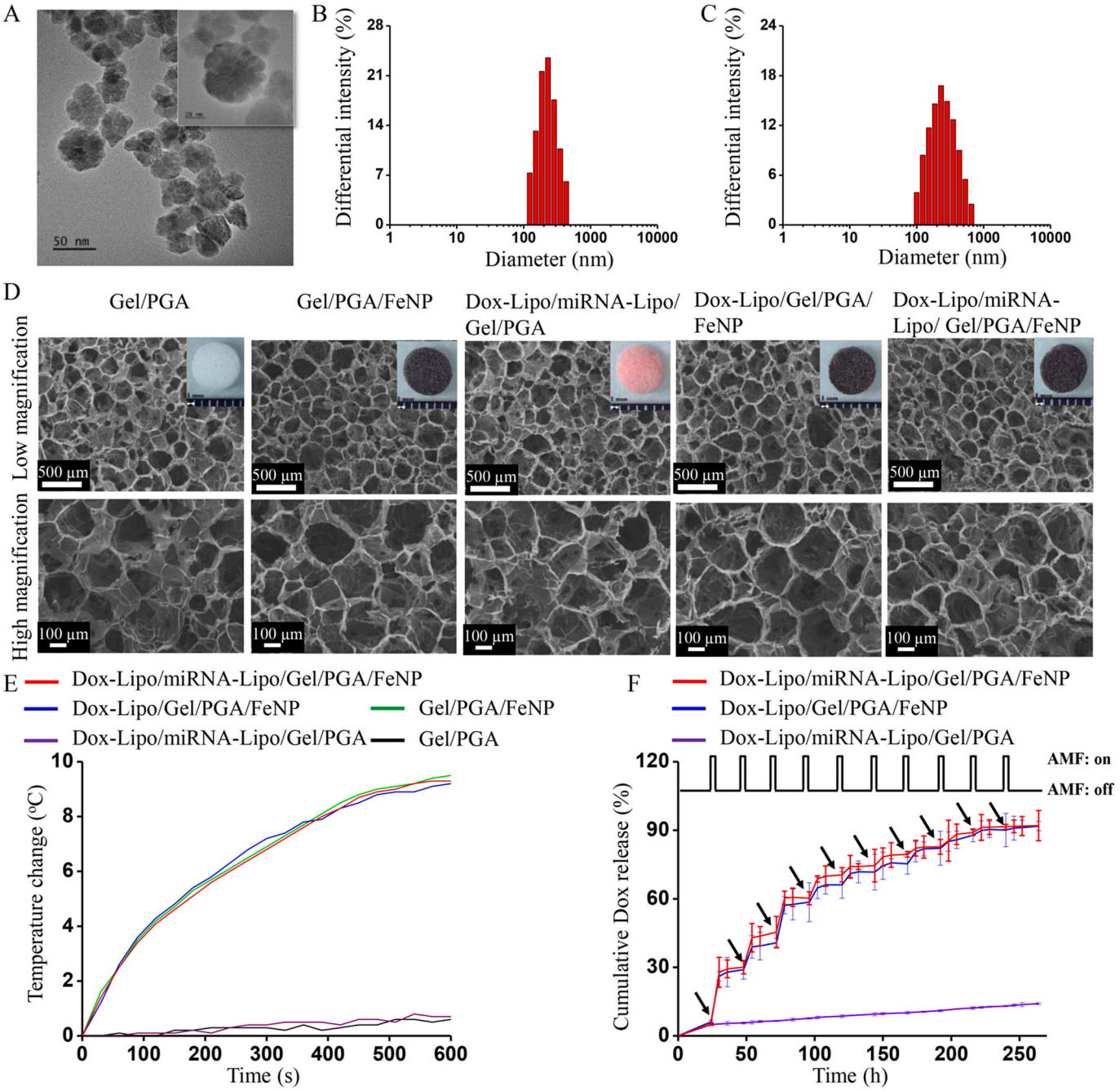

Fig. 1. Characterization of Fe_3O_4 NPs, liposomes and composite scaffolds. (A) TEM image of Fe_3O_4 NPs. The inserted image is an enlargement of Fe_3O_4 NPs. Hydrodynamic size distribution of (B) Dox/DPPC/Chol/DSPE liposomes and (C) miRNA/DOPE/CHEMS/DSPE liposomes. (D) SEM image of scaffolds. The inserted image is gross appearance of composite scaffolds. (E) Temperature change curve of scaffolds under AMF irradiation for 10 min (frequency: 373.6 kHz; field: 100 Gauss). (F) Thermosensitive release profile of Dox from Dox-loaded scaffolds during incubation in 37 °C PBS with a periodic switching on and off of AMF irradiation for 10 min. The arrows show time points when AMF was switched on. Data are expressed as the means ± S.D (n = 3).

was used to analyze multiple groups. p values less than 0.05 were considered to indicate significant differences.

3. Results

3.1. Characterization of Fe_3O_4 NPs and liposomes

The shape and size of the Fe_3O_4 NPs were characterized by transmission electron microscopy (TEM). TEM images (Fig. 1A) revealed that the Fe_3O_4 NPs had a flower-like shape with an average size of 33.2 ± 5.9 nm. The hydrodynamic size of Fe_3O_4 NPs was measured by dynamic light scattering (DLS). The Fe_3O_4 NPs had an average size of 107.8 ± 47.6 nm in aqueous solution (Fig. S3), which confirmed the high dispersibility of the NPs. The hydrodynamic sizes of Dox/DPPC/Chol/DSPE liposomes (Dox-Lipo) and miRNA/DOPE/CHEMS/DSPE liposomes (miRNA-Lipo) were analyzed by DLS. As shown in Fig. 1B and C, Dox-Lipo and miRNA-Lipo displayed uniform size distributions of 225.3 ± 68.9 nm and 279.4 ± 141.6 nm, respectively. The sizes of both types of liposomes were well controlled by the thin-film hydration method and did not change significantly after the encapsulation of Dox or miRNA (Figs. S4 and S5). The encapsulation efficiencies of Dox-Lipo and miRNA-Lipo, which were calculated by measuring the fluorescence of Dox and miRNA (labeled with Cy5) after destroying the liposomes, were 42.8 ± 5.6 % and 63.8 ± 4.3 %, respectively (Tables S1 and S2).

3.2. Scaffold characterization

The multifunctional composite scaffolds (Dox-Lipo/miRNA-Lipo/Gel/PGA/FeNP) were fabricated by immobilizing Dox-Lipo and miRNA-Lipo in the porous scaffolds of Fe_3O_4 NPs, Gel and PGA. Porous scaffolds of Fe_3O_4 NPs, Gel and PGA (Gel/PGA/FeNP) were fabricated using ice microparticles with a diameter of 250–355 μm as a porogen material to construct pore structures. The Dox-Lipo was immobilized in the porous scaffolds via the coupling of amino groups in the liposomes to carboxyl groups in the porous scaffolds. The miRNA-Lipo was conjugated in the porous scaffolds by a click reaction between azide groups in the MMP-7 cleavable peptide modified on the liposomes and BCN groups in the porous scaffolds (Fig. S6). As controls, porous scaffolds of Gel and PGA without Fe_3O_4 NPs (Gel/PGA), Gel/PGA scaffolds immobilized with Dox-Lipo and miRNA-Lipo (Dox-Lipo/miRNA-Lipo/Gel/PGA) and Gel/PGA/FeNP scaffolds immobilized with Dox-Lipo (Dox-Lipo/Gel/PGA/FeNP) were also fabricated. All the scaffolds had similar large, spherical pores because the same ice microparticles were used in the scaffold preparation processes. The pore sizes of the scaffolds ranged from 250 to 355 μm. In addition, there were some small pores on the walls of the large pores that endowed the scaffolds with good interconnectivity (Fig. 1D). The magnetic properties of the Fe_3O_4 NPs in the composite scaffold were measured. As shown in Fig. S7, the normalized field-dependent magnetization (M − H) curves of the free Fe_3O_4 NPs and the Fe_3O_4 NPs in the composite scaffolds exhibited no hysteresis with good reversibility at 300 K. Both the free Fe_3O_4 NPs and the Fe_3O_4 NPs in the composite scaffolds had superparamagnetic properties at room temperature. The saturation magnetization of free Fe_3O_4 NPs and the Fe_3O_4 NPs in the composite scaffolds was 63.0 emu/g and 44.8 emu/g, respectively. The composite scaffolds with superparamagnetic NPs had an effect on the magnetic dipole interactions between them, resulting in the weakened overall saturation magnetization [60]. The loading efficiencies of Dox-Lipo in the Dox-Lipo/miRNA-Lipo/Gel/PGA, Dox-Lipo/Gel/PGA/FeNP and Dox-Lipo/miRNA-Lipo/Gel/PGA/FeNP composite scaffolds were 50.4 ± 4.9 %, 53.6 ± 7.5 % and 51.9 ± 6.6 %, respectively (Table S3). The loading efficiencies of miRNA-Lipo in the Dox-Lipo/miRNA-Lipo/Gel/PGA and Dox-Lipo/miRNA-Lipo/Gel/PGA/FeNP composite scaffolds were 43.0 ± 3.7 % and 42.2 ± 5.5 %, respectively, maintaining good consistency in each production (Table S4).

The biostability of the scaffolds was assessed through both *in vitro* and *in vivo* degradation experiments. For the *in vitro* degradation experiments, the Gel/PGA (control) and Dox-Lipo/miRNA-Lipo/Gel/PGA/FeNP composite scaffolds were immersed in PBS with or without 50 μg/mL collagenase at 37 °C. As shown in Fig. S8A, the weight of the composite scaffolds remained constant when they were immersed in PBS without collagenase for a two-week period, indicating their stability during incubation with no signs of degradation. However, in the presence of collagenase (Fig. S8B), the composite scaffolds could be degraded. The scaffold weight gradually decreased over time and eventually reached zero after one week of incubation. Although complete degradation of the scaffolds occurred within one week in the collagenase-containing solution, notably, the collagenase concentration used in this experiment (50 μg/mL) greatly exceeded its typical concentration in the normal physiological environment (1.6–24.0 ng/mL) [61]. For the *in vivo* degradation experiments, cancer cells were seeded in the Dox-Lipo/miRNA-Lipo/Gel/PGA/FeNP composite scaffolds, and then the cell/scaffolds were implanted in the dorsal regions of the mice. On Days 14 and 28 after AMF irradiation, the implanted composite scaffolds were retrieved for observation. As shown in Fig. S9, the composite scaffolds maintained their structural integrity and size at both the two- and four-week time points, further demonstrating the stability of the scaffolds during *in vivo* implantation.

The magnetic thermal properties of the scaffolds were measured by applying AMF. During AMF irradiation, the temperatures of the Gel/PGA and Dox-Lipo/miRNA-Lipo/Gel/PGA scaffolds changed only slightly within 10 min, which resulted in no heat conversion capability, whereas the temperatures of the Gel/PGA/FeNP, Dox-Lipo/Gel/PGA/FeNP and Dox-Lipo/miRNA-Lipo/Gel/PGA/FeNP composite scaffolds increased quickly during AMF irradiation (Fig. 1E). The temperature changes of the Gel/PGA/FeNP, Dox-Lipo/Gel/PGA/FeNP and Dox-Lipo/miRNA-Lipo/Gel/PGA/FeNP composite scaffolds were 9.3 ± 0.4 °C, 9.0 ± 0.5 °C and 9.1 ± 0.2 °C, respectively. These results suggested that the scaffolds incorporated with Fe_3O_4 NPs had good magnetic thermal conversion properties and that there was no noticeable difference in heat conversion capability before and after liposome loading.

3.3. Magnetic hyperthermia-controlled Dox release

The temperature-dependent Dox release from Dox-Lipo-loaded composite scaffolds was investigated during periodic AMF irradiation. Dox was only released from the DPPC liposomes when the temperature reached the phase transition temperature of the liposomes. No mechanical stress acting on the scaffold affected the release of Dox. As shown in Fig. 1F and Fig. S10, the Dox-Lipo-loaded composite scaffolds without AMF irradiation exhibited very low release of Dox. After 11 days of incubation in PBS at 37 °C, the release rates of Dox from the Dox-Lipo/miRNA-Lipo/Gel/PGA, Dox-Lipo/Gel/PGA/FeNP and Dox-Lipo/miRNA-Lipo/Gel/PGA/FeNP composite scaffolds were 14.9 ± 0.5 %, 15.1 ± 0.3 % and 13.6 ± 0.4 %, respectively. When the Dox-Lipo-loaded composite scaffolds were irradiated with AMF, the release of Dox increased rapidly. After the first cycle of AMF irradiation, 27.9 ± 6.4 % and 29.3 ± 3.9 % of the Dox was released from the Dox-Lipo/Gel/PGA/FeNP and Dox-Lipo/miRNA-Lipo/Gel/PGA/FeNP composite scaffolds, respectively. During consecutive AMF-on and AMF-off cycles, the release of Dox accelerated quickly when the AMF was on but decelerated once the AMF was off. The cumulative amounts of Dox released from the Dox-Lipo/Gel/PGA/FeNP and Dox-Lipo/miRNA-Lipo/Gel/PGA/FeNP composite scaffolds after 10 cycles of AMF irradiation were 91.8 ± 2.1 % and 92.0 ± 6.6 %, respectively. In contrast, the Dox-Lipo/miRNA-Lipo/Gel/PGA scaffolds still resulted in very slow Dox release when irradiated by AMF.

3.4. MMP-7-specific cleavage to release miRNA-Lipo from composite scaffolds and cancer cell uptake of miRNA-Lipo

The release property of miRNA-Lipo cleaved by MMP-7 from the

composite scaffolds was evaluated using Dox-Lipo/miRNA-Lipo/Gel/PGA/FeNP composite scaffolds with MMP-7 enzyme treatment. As shown in Fig. 2A, in the absence of MMP-7, the amount of miRNA-Lipo released from the composite scaffolds after 12 h of incubation was very low. In contrast, 48.8 ± 4.9 % and 67.3 ± 7.1 % of the miRNA-Lipo was released from the composite scaffolds after incubation with MMP-7 for 2 and 12 h, respectively. These results suggested that the MMP-7-responsive release of miRNA-Lipo from the composite scaffolds could be achieved by the use of specific MMP-7-cleavable peptides as linkers between the liposomes and the scaffolds.

The cellular uptake of miRNA-Lipo cleaved from the composite scaffolds was investigated by incubating Dox-tolerant MDA-MB-231 cells with Dox-Lipo/miRNA-Lipo/Gel/PGA/FeNP composite scaffolds and observing the results by confocal laser scanning microscopy. After 1 day of coculture, a strong red fluorescence signal was detected in the cells, and the red fluorescence was strongly colocalized in the lysosomes (Fig. 2B). The miRNA-Lipo/Gel/PGA scaffolds were also used to further demonstrate the release properties of miRNA-Lipo (Fig. S11). The Pearson correlation coefficients between the red and green channels in Fig. 2B and S11B were 0.837 and 0.723, respectively, indicating a strong positive correlation between the two channels. These results showed that the miRNA-Lipo could be precisely cleaved and released from the miRNA-Lipo-loaded composite scaffolds under MMP-7 treatment and further endocytosed by Dox-tolerant MDA-MB-231 cells. Furthermore, we investigated the chemosensitization effect of miRNA (miR-200c) on Dox-resistant MDA-MB-231 cells. As shown in Fig. S12, the IC_{50} in the miRNA-Lipo-treated cells decreased to 1.4 μM compared with that in the control cells (IC_{50} = 3.2 μM). This confirmed that miRNA (miR-200c) had a significant chemosensitizing effect on drug-resistant breast cancer cells.

3.5. *Synergistic anticancer effects of multifunctional composite scaffolds on Dox-tolerant MDA-MB-231 cells*

The synergistic therapeutic effect of magnetic hyperthermia and sensitizing chemotherapy of the composite scaffolds was studied using Transwell plates. Dox-tolerant MDA-MB-231 cells were seeded in the scaffolds and in the bottom wells of Transwell plates. The cells/scaffolds placed in the inserts of the Transwell plates were irradiated with AMF for 10 min and then returned to the inserts for further incubation at 37 °C. AMF irradiation was performed every 24 h for a total of three times. The viability of Dox-tolerant MDA-MB-231 cells in the scaffolds after each AMF irradiation was evaluated by live/dead staining (Fig. 3 and S13). Before AMF irradiation, green fluorescence was observed for the breast cancer cells in all the scaffolds, and almost no red fluorescence was observed, indicating that all the cells were alive.

In the Gel/PGA scaffold group, all the cells survived after three cycles of AMF irradiation, indicating that the Gel/PGA scaffolds had no anticancer effect. Some cells in the Gel/PGA/FeNP composite scaffolds died after AMF irradiation because of its magnetic hyperthermia effect. The number of red fluorescent dots in the Dox-Lipo/miRNA-Lipo/Gel/PGA scaffolds constantly increased with time, which was due to the gradual death of the cells caused by the slow release of Dox. Most cells in the Dox-Lipo/Gel/PGA/FeNP composite scaffolds died after three cycles of AMF irradiation, and only a few live cells were detected, which showed that the synergistic effect of magnetic hyperthermia and chemotherapy killed most but not all of the Dox-tolerant MDA-MB-231 cells. In contrast, in the Dox-Lipo/miRNA-Lipo/Gel/PGA/FeNP composite scaffolds, all Dox-tolerant MDA-MB-231 cells died because miRNA could reduce Dox resistance and increase the sensitization of cancer cells to Dox to enhance the anticancer effect.

Moreover, quantitative analysis revealed that the viability of the breast cancer cells in the Gel/PGA scaffolds was unchanged before and after AMF irradiation (Fig. 4A). After three cycles of AMF irradiation, the viability of the cells in the Gel/PGA/FeNP composite scaffolds decreased to 45.1 ± 9.4 %. The viability of the cells cultured in the Dox-Lipo/miRNA-Lipo/Gel/PGA/FeNP composite scaffolds decreased the most significantly to 3.5 ± 4.3 %. The results indicated that the synergistic effect of magnetic hyperthermia and sensitizing chemotherapy of the Dox-Lipo/miRNA-Lipo/Gel/PGA/FeNP composite scaffolds most efficiently killed the Dox-tolerant MDA-MB-231 cells in the scaffolds.

The viability of the cells in the bottom wells of the transwell plates was also quantified (Fig. 4B). After three cycles of AMF irradiation, the viabilities of the cells cultured in the bottom wells incubated with the Gel/PGA and Gel/PGA/FeNP composite scaffolds were not significantly different. The viability of the Dox-tolerant MDA-MB-231 cells in the bottom wells incubated with the Dox-Lipo/miRNA-Lipo/Gel/PGA composite scaffolds was lower than those in the bottom wells incubated with the Gel/PGA and Gel/PGA/FeNP composite scaffolds, a difference that was due to the slow release of Dox, which induced the death of some cells. The viability of the cells in the bottom wells incubated with the Dox-Lipo/Gel/PGA/FeNP composite scaffolds continuously decreased to a very low level as the number of AMF irradiation increased. The viability of the cells in the bottom wells incubated with the Dox-Lipo/miRNA-Lipo/Gel/PGA scaffolds was the lowest. Statistical analysis of the scaffolds and bottom wells at each time of AMF irradiation was performed to assess differences between groups. As shown in Fig. S14, cell viability in the Dox-Lipo/miRNA-Lipo/Gel/PGA/FeNP composite scaffolds was significantly lower than that in the other types of scaffolds. The viability of the cells in the bottom wells of the Dox-Lipo/miRNA-Lipo/Gel/PGA/FeNP composite scaffold group was also significantly lower than that of the other groups. The results showed that the Dox-Lipo/miRNA-Lipo/Gel/PGA/FeNP composite scaffold efficiently eliminated Dox-tolerant MDA-MB-231 cells after AMF irradiation because of the increased sensitization of drug-tolerant cancer cells and the synergistic effect of magnetic hyperthermia and sensitizing

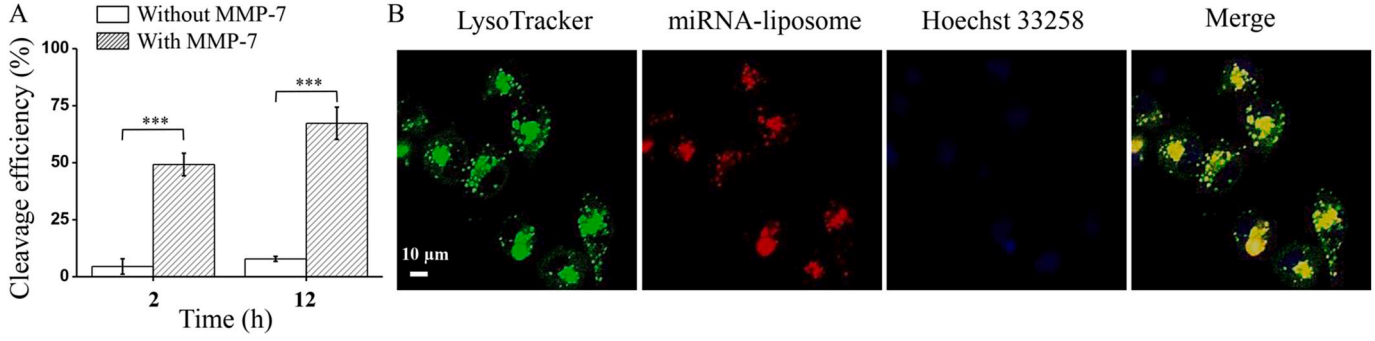

Fig. 2. MMP-7 cleavage-controlled release of miRNA-Lipo. (A) The cleavage efficiency of miRNA-Lipo from Dox-Lipo/miRNA-Lipo/Gel/PGA/FeNP composite scaffolds after 2 h and 12 h of incubation with or without MMP-7 enzyme. (B) Confocal fluorescence imaging of Dox-tolerant MDA-MB-231 cells for visualizing the co-localization of lysosomes and miRNA-Lipo region after cells incubated with Dox-Lipo/miRNA-Lipo/Gel/PGA/FeNP composite scaffolds. Green: lysosomes, red: miRNA-Lipo, blue: nucleus. Data are expressed as the means ± S.D (n = 3). Significant difference: ***$p < 0.001$.

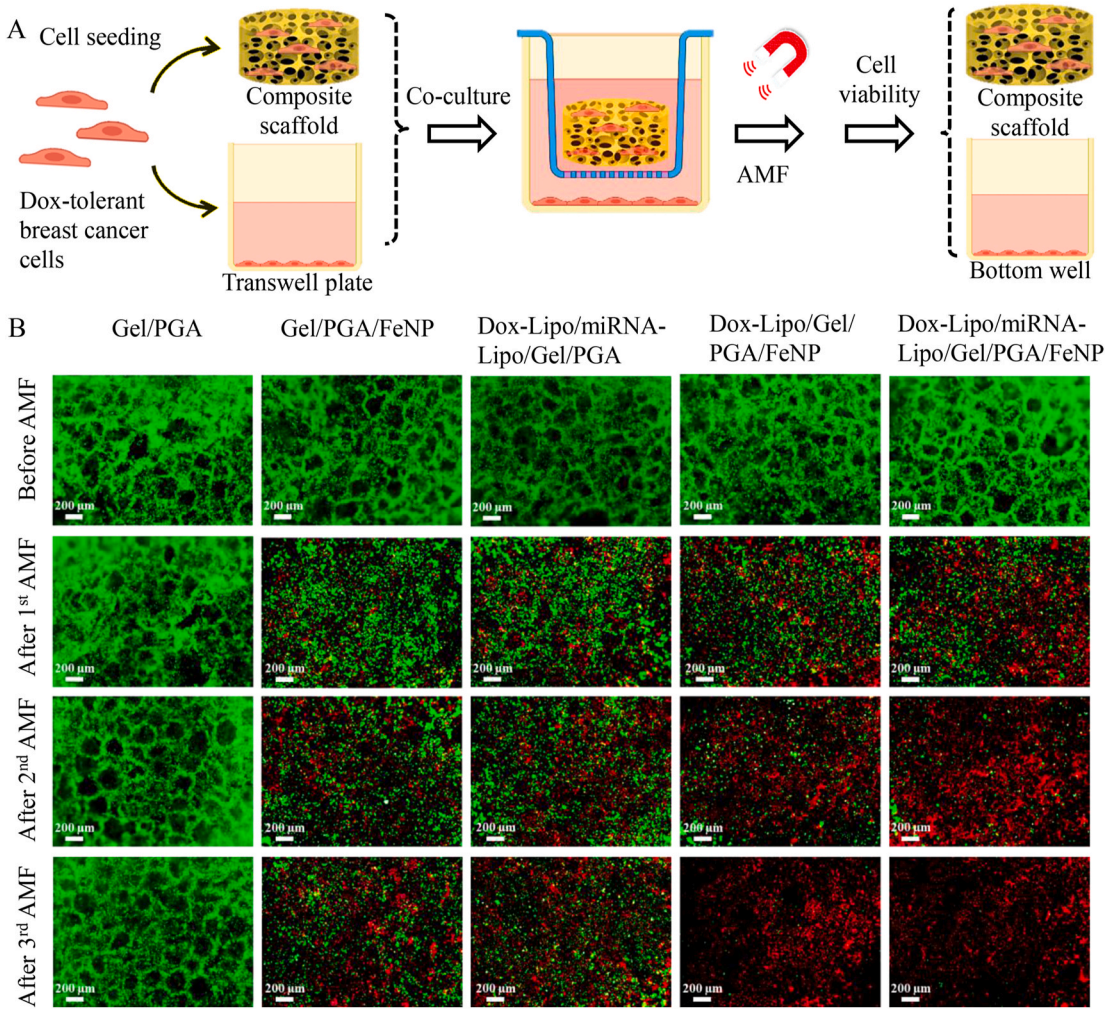

Fig. 3. *In vitro* synergistic anticancer effect of composite scaffolds against Dox-tolerant MDA-MB-231 cells. (A) Schematic illustration of the cell experimental procedure. (B) Live/dead staining of cells cultured in scaffolds before and after AMF irradiation. Living and dead cells were stained green and red, respectively.

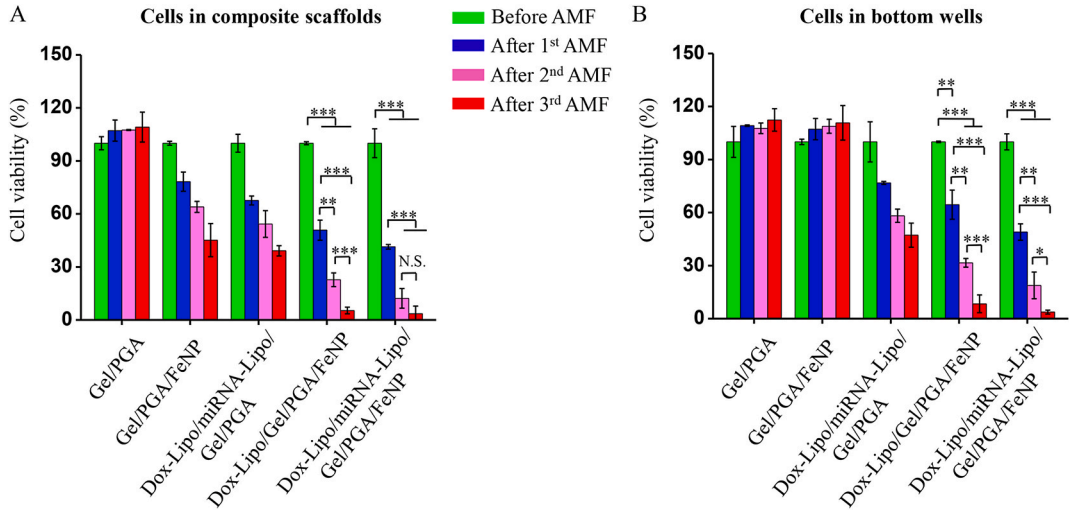

Fig. 4. Quantification of cell viability. Viability of Dox-tolerant MDA-MB-231 cells in (A) scaffolds and (B) bottom wells before and after three times of AMF irradiation at a field intensity of 100 Gauss for 10 min. Data are expressed as the means ± S.D. (n = 3). Significant difference: *p < 0.05, **p < 0.01, ***p < 0.001. N. S.: no significant difference.

chemotherapy.

3.6. *In vivo* synergistic therapeutic effects of the composite scaffolds

After confirming the *in vitro* anticancer effect, an animal experiment was performed to investigate the synergistic anticancer effect against drug-tolerant breast cancer cells. *In vivo* tumor killing experiments (Fig. 5) were performed one day after implantation because the cancer cells were seeded in the scaffolds before implantation to simulate the residual cancer cells that migrated in the scaffolds. Dox-tolerant MDA-MB-231 cells were seeded on the scaffolds (Gel/PGA, Gel/PGA/FeNP, Dox-Lipo/miRNA-Lipo/Gel/PGA, Dox-Lipo/Gel/PGA/FeNP and Dox-Lipo/miRNA-Lipo/Gel/PGA/FeNP). The donut-shaped scaffold rings of Gel/PGA were seeded with cancer cells to test the sensitizing chemotherapeutic effect of the released miRNA-Lipo and Dox, which were similar to those in the bottom wells of the Transwell plates. The cells/scaffolds were placed inside the scaffold rings and subcutaneously implanted together in the backs of nude mice. The cancer cells in the donut-shaped porous scaffold rings could well model the residual cancer cells outside of the scaffolds. After implantation, the mice were irradiated with AMF for 10 min, and the local skin temperature in the implanted area was recorded during AMF irradiation. Before and after each AMF irradiation, the viability of cells within the scaffolds and scaffold rings was evaluated by measuring bioluminescence with an *in vivo* vision system (IVIS).

The mice implanted with various cell/scaffold constructs exhibited distinct responses to AMF irradiation. As shown in Fig. S15, in the case of the cell/Gel/PGA and cell/Dox-Lipo/miRNA-Lipo/Gel/PGA constructs,

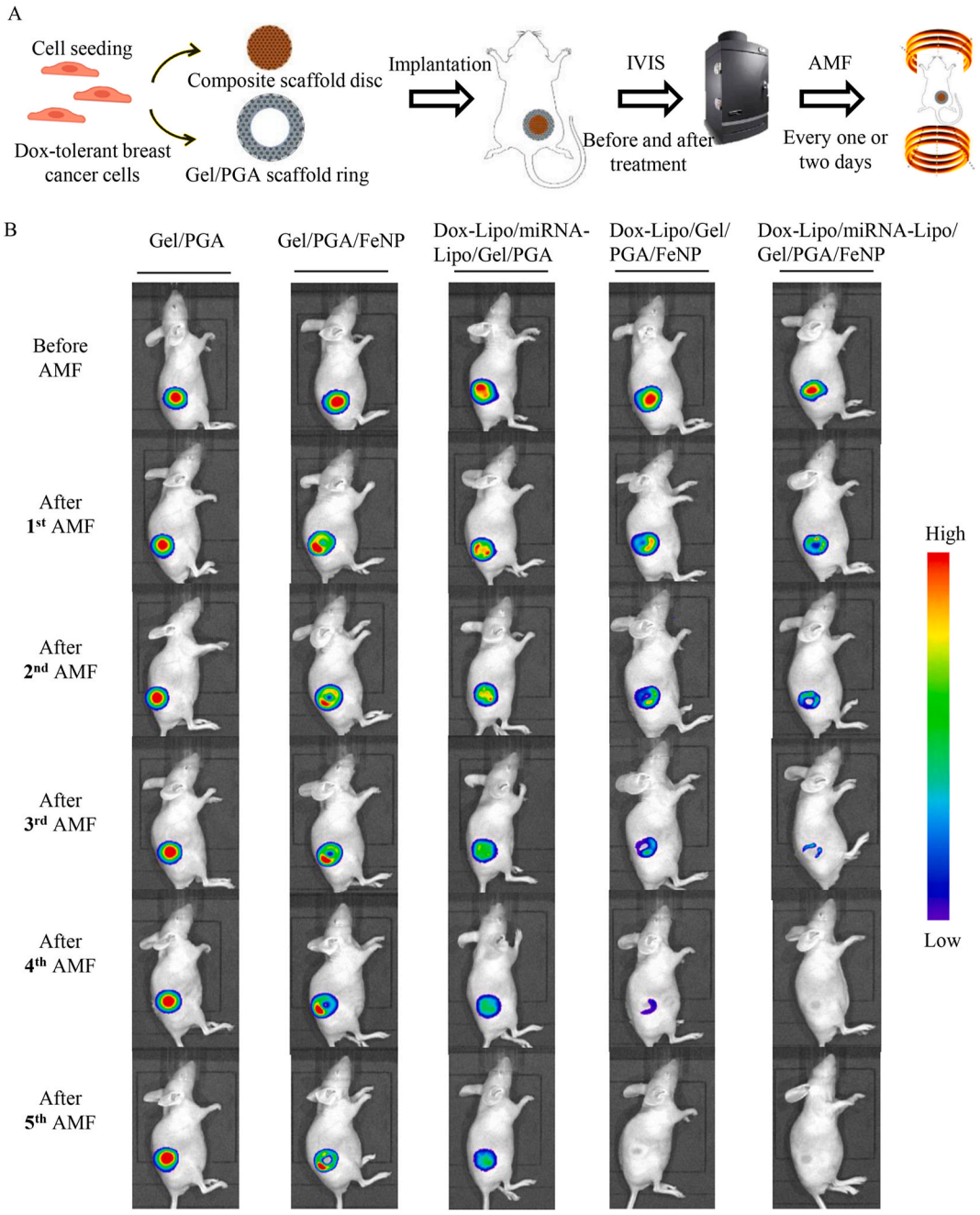

Fig. 5. *In vivo* bioluminescence monitoring. (A) Schematic representation and timeline of *in vivo* animal experiment. (B) Whole-body bioluminescence image of mice before and after AMF treatment.

gradual declines in local skin temperature were observed. This phenomenon could be attributed to the normal anesthesia-induced physiological cooling of the anesthetized mice [54], which indicated that the local skin did not experience significant heating during AMF irradiation. However, when mice implanted with the cell/Gel/PGA/FeNP, cells/Dox-Lipo/Gel/PGA/FeNP and cell/Dox-Lipo/Lipo/Gel/PGA/FeNP constructs were irradiated by AMF, their local skin temperature increased to 42.7 °C, 42.6 °C and 42.8 °C, respectively. These results suggested the excellent magnetothermal conversion capability of the implanted composite scaffolds. During AMF irradiation, the composite scaffolds could generate a mild magnetic hyperthermia environment that surpassed the lipid phase transition temperature to disturb the liposome bilayers to accelerate Dox release from the Dox-Lipo.

Whole-body bioluminescence imaging revealed a strong bioluminescence signal on the dorsal side of each mouse before AMF irradiation, confirming the viability of Dox-tolerant MDA-MB-231 cells in all the scaffolds following implantation (Fig. 5B and Fig. S16). The mice implanted with the cells/Gel/PGA constructs exhibited strong bioluminescent signals even after five cycles of AMF irradiation. The results of the quantitative bioluminescence analysis (Fig. S17A) revealed that the post-irradiation value was 1.4 times greater than the initial value, implying that Gel/PGA did not have any anticancer effect and that the cancer cells were able to grow within the scaffolds. The mice implanted with the cell/Gel/PGA/FeNP constructs exhibited a decreasing trend in the bioluminescence signal with periodic AMF irradiation. After five cycles of AMF irradiation, the bioluminescence signal in the central regions became very low but remained robust within the donut-shaped scaffold rings. These results suggested that the hyperthermia generated within the central Gel/PGA/FeNP scaffolds could gradually eliminate breast cancer cells, whereas cancer cells located in the donut-shaped scaffold rings remained unaffected by the treatment.

For the mice implanted with the cell/Dox-Lipo/miRNA-Lipo/Gel/PGA constructs, the bioluminescence signals became weaker both in the central scaffolds and the outer scaffold rings over time. These decreases in the bioluminescence signals were attributed to the gradual release of miRNA-Lipo and Dox, which led to cell death. For the mice implanted with the cell/Dox-Lipo/Gel/PGA/FeNP constructs, the bioluminescence signal in the central scaffold disappeared after three cycles of AMF irradiation, and the bioluminescence signal in the surrounding scaffold rings weakened after each AMF irradiation and eventually vanished after five cycles of AMF irradiation. This occurred because the Dox-Lipo/Gel/PGA/FeNP composite scaffolds had synchronous magnetic hyperthermia and chemotherapy effects on cancer cells inside the scaffolds and chemotherapy effect inside the scaffold rings. However, when the mice implanted with the cell/Dox-Lipo/miRNA-Lipo/Gel/PGA/FeNP constructs were irradiated with AMF, the bioluminescent signals in both the central scaffolds and surrounding scaffold rings decreased faster, disappeared in the central scaffolds after two cycles of AMF irradiation and disappeared in the scaffold rings after four cycles of AMF irradiation. This was attributed to the cleavable release of MMP-7 from the miRNA-Lipo loaded in the composite scaffolds, which reduced the drug resistance of the cancer cells. When combined with synchronous magnetic hyperthermia and chemotherapy, this synergistic strategy has more effective anticancer effects on drug-tolerant breast cancer cells. The results indicated that Dox-tolerant MDA-MB-231 cells in the central scaffolds of Dox-Lipo/miRNA-Lipo/Gel/PGA/FeNP and in the peripheral scaffold rings were most effectively eliminated due to the synergistic effect of magnetic hyperthermia and sensitizing chemotherapy. Additionally, the survival rates of the mice in all the experimental groups during the *in vivo* anticancer experiment are shown in Fig. S17B. No mouse fatality was observed, and there was no significant difference in mouse survival rates among all the groups. The images of scaffold implantation after treatment are shown in Fig. S17C. At 4 weeks after treatment, the implanted scaffold rings and scaffold discs could be clearly observed.

3.7. In vivo biosafety of the composite scaffolds

The biosafety of the composite scaffolds was assessed both during and after anticancer treatment. We examined the metabolism and distribution of Fe_3O_4 NPs in mice on Days 1 and 14 after anticancer treatment by ICP−OES. H&E staining of several major organs was also performed to evaluate the biosafety of the strategy. As shown in Fig. S18, ICP−OES analysis revealed that the levels of iron in various organs and in the blood of mice implanted with the Dox-Lipo/miRNA-Lipo/Gel/PGA/FeNP composite scaffold did not significantly differ from those in the control group. Furthermore, the H&E staining results (Fig. S19) revealed no noticeable differences between the mice implanted with the Dox-Lipo/miRNA-Lipo/Gel/PGA/FeNP composite scaffolds and those implanted with the control scaffolds (Gel/PGA). The results indicated that the composite scaffolds had good biosafety following *in vivo* implantation.

3.8. Promotion of hMSC proliferation and adipogenesis

In addition to their use in anticancer treatment, the composite scaffolds after the release of all the miRNA-Lipo and Dox could be utilized to guide new tissue regeneration. To evaluate the ability of the Dox-Lipo/miRNA-Lipo/Gel/PGA/FeNP composite scaffolds to regenerate adipose tissue, the composite scaffolds were treated with MMP-7 and AMF to fully release the loaded miRNA-Lipo and Dox. Then, hMSCs were seeded in the composite scaffolds, and the proliferation and adipogenesis of the hMSCs were evaluated. As shown in Fig. 6A and S20, all the hMSCs were alive after 1 day of culture, indicating that the hMSCs retained good viability in the scaffolds. The cell distribution in the scaffolds was evaluated by staining the cell nuclei in the cell/scaffold constructs with DAPI. The results in Fig. 6B revealed that the hMSCs were evenly distributed throughout the scaffolds because of the highly porous and interconnected structure of the scaffolds. Moreover, SEM images (Fig. S21) further revealed that hMSCs adhered well to the pore walls and spread well in the scaffolds. The DNA content in the scaffolds was measured to analyze the hMSC proliferation after 1, 3, 5 and 7 days. As shown in Fig. 6C, the DNA content increased in a time-dependent manner, which suggested that the composite scaffolds promoted the proliferation of hMSCs. Additionally, the effect of miR-200c/liposomes on MSCs was studied. As shown in Fig. S22, there was no significant effect on MSCs.

Lipid droplet staining and gene expression analysis were utilized to evaluate the adipogenesis of hMSCs in the scaffolds. In the absence of adipogenesis-inducing medium, no noticeable oil droplets were observed in either scaffold (Fig. 7A). However, upon culture in adipogenesis-inducing medium, clear oil droplets were observed in both scaffolds. There was no significant difference in oil droplet staining between the Dox-Lipo/miRNA-Lipo/Gel/PGA/FeNP and Gel/PGA scaffolds (Fig. 7B). Gene expression analysis revealed that the expression levels of adipogenesis-related genes (FASN, FABP4, CEBPA and LPL) were low when the hMSC/scaffold constructs were cultured in basal medium. However, the expression levels of these genes were significantly upregulated in adipogenic medium (Fig. 7C and D). Moreover, there was no significant difference in gene expression between the two types of scaffolds. These results indicated that after drug release, the composite scaffolds were able to support the adipogenesis of hMSCs and had potential in adipose tissue reconstruction.

3.9. In vivo promoting effect on tissue regeneration

The *in vivo* tissue regeneration capacity of the multifunctional composite scaffolds was evaluated after eliminating cancer cells. Breast cancer cells were seeded in the Dox-Lipo/miRNA-Lipo/Gel/PGA/FeNP composite scaffolds, and the cell/scaffold constructs were subcutaneously implanted in the dorsal regions of mice, followed by AMF irradiation. On Days 14 and 28 after AMF irradiation, the scaffolds were

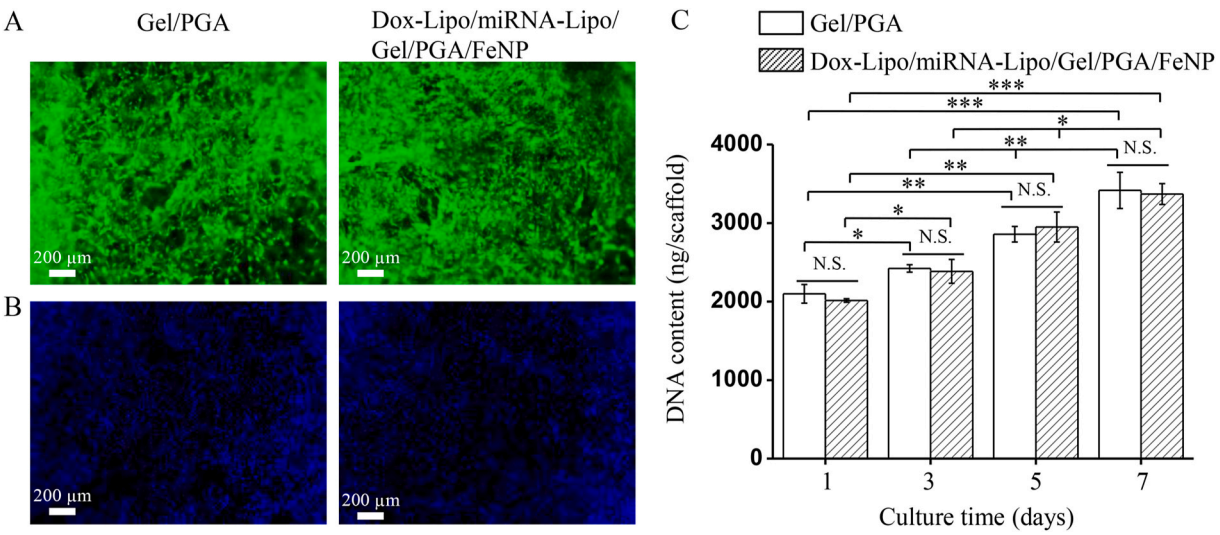

Fig. 6. Effect of composite scaffolds on activity of hMSCs after drug release. (A) Live/dead staining of hMSCs cultured in scaffolds for 1 day. Living and dead cells were stained green and red, respectively. (B) Nuclear staining of hMSCs cultured in scaffolds for 1 day. Cell nucleus was stained blue. (C) DNA content of hMSCs/scaffold constructs after 1, 3, 5 and 7 days of culture. Data are expressed as the means ± S.D. (n = 3). Significant difference: *p < 0.05, **p < 0.01, ***p < 0.001. N.S.: no significant difference.

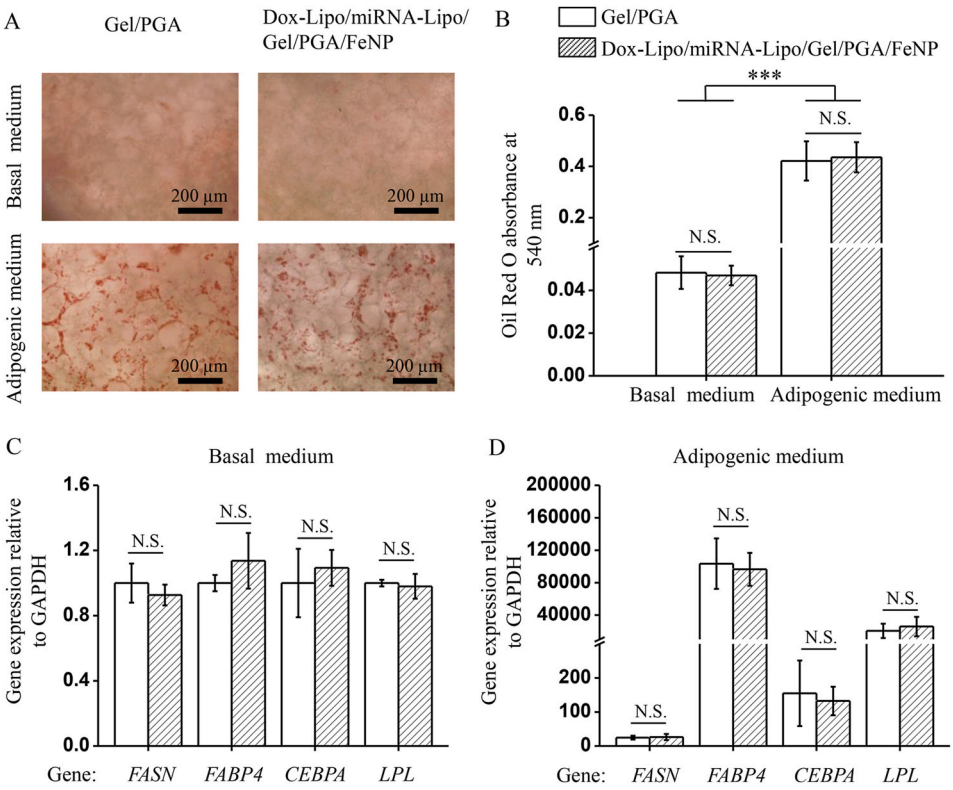

Fig. 7. Adipogenic differentiation of hMSCs cultured in composite scaffolds after drug release. (A) Lipid droplet staining with oil red O dye. (B) Quantification of stained lipid droplets of hMSCs/scaffold constructs cultured in basal and adipogenic medium for 21 days. Quantitative analysis of the expression levels of FASN, FABP4, CEBPA and LPL of hMSCs cultured in the scaffolds in (C) basal and (D) adipogenic medium for 21 days. Data are presented as the means ± S.D. (n = 3). Significant difference: ***p < 0.001. N.S.: no significant difference.

retrieved, and H&E staining was conducted to investigate the migration of normal cells into the scaffolds. As shown in Fig. S23, cell nuclei and extracellular matrices were detected within the scaffolds on Day 14 after AMF irradiation. On Day 28, notable increases in the number of cell nuclei and cellular matrices were observed. There were no cancer cells in the scaffolds after AMF irradiation because all the cancer cells were killed by the composite scaffolds due to the synergistic effects of magnetic hyperthermia and sensitizing chemotherapy. The positive identification of these cells and cellular matrices suggested that after AMF irradiation, neighboring normal cells had the capacity to migrate and adhere to the composite scaffolds, consequently facilitating the potential for new tissue regeneration.

4. Discussion

Synergistic hyperthermia and chemotherapy has been proposed as a promising treatment modality to achieve a stronger therapeutic effect than monotherapy [34–38]. Recent studies have explored the use of hydrogel scaffold systems for *in situ* delivery of chemotherapy drugs and hyperthermia nanoparticles, combining chemotherapy with hyperthermia [62,63]. These hydrogel systems can enhance therapeutic efficacy by enabling the *in situ* delivery of both drugs and nanoparticles. However, challenges remain, including the inability to precisely and synchronously control drug release during hyperthermia and limitations in combination therapy for drug-resistant tumor cells. In this study, we developed a novel approach by incorporating two types of responsive liposomes into a magnetic composite scaffold for delivering chemotherapy drugs and chemosensitizing miRNAs. One type of liposome is DOPE liposomes, which contain chemosensitizing miRNAs and are attached to the magnetic composite scaffold using tumor microenvironment enzyme-cleavable peptide (-PLGLA-) linkers. The other type is DPPC liposomes loaded with the chemotherapeutic drug Dox, which are anchored to the scaffold through noncleavable amide chemical bonds, allowing for a synchronous response to magnetic hyperthermia. Upon scaffold implantation, MMP-7 overexpressed in the tumor microenvironment can cleave the -PLGLA-linkers, releasing the miRNA/DOPE liposomes. These liposomes are then endocytosed by tumor cells, releasing miRNA into the cytoplasm, downregulating the expression of MDR1 (P-glycoprotein) and reducing drug resistance. Following chemosensitization, alternating magnetic field (AMF) irradiation was applied to heat the scaffold. This heating triggered the release of Dox from the thermosensitive DPPC liposomes, enabling synchronized sensitizing chemotherapy and magnetic hyperthermia treatment of the tumor cells. Additionally, after treatment, the scaffolds facilitated *in situ* tissue repair. Thus, these multifunctional scaffolds not only control the release of multiple therapeutic agents, providing combined magnetic hyperthermia and sensitizing chemotherapy for drug-resistant breast cancer cells, but also support tissue regeneration, addressing several clinical challenges.

Magnetic hyperthermia in cancer therapy is derived from the heat from magnetothermal conversion agents under AMF irradiation and has potential for clinical application in deep-seated cancer. Scaffolds have been utilized to deliver NPs for localized and repeated hyperthermia [26–33]. As shown in Fig. 1E, the composite scaffolds had good magnetic thermal properties under AMF irradiation, and the loaded liposomes did not affect the heating efficiency of the scaffolds. The temperature change of the Dox-Lipo/miRNA-Lipo/Gel/PGA/FeNP composite scaffold after AMF irradiation was 9.1 ± 0.2 °C, which could be used for temperature-controlled Dox release from the Dox-Lipo immobilized in the scaffold.

Dox, a potent chemotherapy drug, is effective at inhibiting cancer cells but is associated with significant disadvantages. Its limitations include severe side effects and a lack of targeted delivery, which may compromise patient safety and therapeutic efficacy. In contrast, hydrogel scaffold systems offer targeted drug delivery, localized treatment, and reduced systemic toxicity [29]. Composite scaffolds used as carriers to transport anticancer drugs for synergistic hyperthermia and chemotherapy have attracted much attention in recent years, but the release of anticancer drugs is uncontrollable and independent of hyperthermia [64,65]. Composite scaffolds can synchronize magnetic hyperthermia and chemotherapy using thermosensitive liposomes to load anticancer drugs. The Dox-Lipo/miRNA-Lipo/Gel/PGA/FeNP composite scaffold showed a high loading efficiency of 51.9 ± 6.6 % and very slow release of Dox without AMF irradiation, which was 13.6 ± 0.4 % when incubated at 37 °C for 11 days (Fig. S10). In contrast, during periodic AMF irradiation, the Dox-Lipo/miRNA-Lipo/Gel/PGA/FeNP composite scaffolds exhibited accelerated Dox release, with a total Dox release of 92 % after 10 cycles of AMF irradiation (Fig. 1F), which indicated that as long as the temperature of the composite scaffolds reached the phase transition temperature of DPPC lipids (41–42 °C) under AMF irradiation, the thermosensitive liposomes would be commanded to release Dox from the composite scaffolds. The composite scaffolds could generate a hyperthermia environment for hyperthermia ablation in cancer cells and trigger the release of Dox encapsulated in thermosensitive DPPC liposomes.

The sensitization of cancer cells and reduction of their drug resistance are important in combination chemotherapy [41,42]. Intratumoral delivery of miRNA-encapsulated liposomes using specific stimuli in the tumor microenvironment, such as MMP-7, is a novel approach to precisely release miRNA-Lipo to drug-tolerant breast cancer cells. The composite scaffolds were capable of cancerous microenvironment-responsive release of miRNA due to the cleavage of the MMP-7-cleavable peptide, which connected the miRNA-encapsulated liposomes to the scaffolds. The Dox-Lipo/miRNA-Lipo/Gel/PGA/FeNP composite scaffolds had a high loading efficiency of miRNA-Lipo (42.2 ± 5.5 %) through a click reaction between azide groups in the MMP-7-cleavable peptides on the miRNA-Lipo and BCN groups in the scaffolds. The composite scaffolds released 67.3 ± 7.1 % of the miRNA-Lipo after 12 h of incubation with MMP-7 (Fig. 2A). The miRNA-Lipo could be precisely released from the composite scaffolds by specific MMP-7 cleavage and endocytosed by Dox-tolerant MDA-MB-231 cells for drug resistance-related gene inhibition (Fig. 2B).

Through the synchronization of magnetic hyperthermia and temperature-controlled release of anticancer drugs from thermosensitive liposomes in combination with the drug resistance suppression effect of miRNAs, the composite scaffolds showed synergistic anticancer effects on Dox-tolerant MDA-MB-231 cells. As shown in Figs. 3–5, the Dox-Lipo/miRNA-Lipo/Gel/PGA/FeNP composite scaffolds showed excellent synergistic anticancer effects to efficiently kill Dox-tolerant MDA-MB-231 both inside and away from the scaffolds. The efficient killing effect was attributed to the reduction in drug resistance induced by the MMP-7-cleavable miRNA-Lipo and the synchronous hyperthermia and chemotherapy effects of the composite scaffolds. In addition, during the anticancer treatment process, the composite scaffolds had no negative side effects on normal tissues or organs. As shown in Figs. S18 and S19, on Days 1 and 14 after AMF irradiation, there was no significant difference in the iron content or tissue status within the major organ tissues of the mice compared with those of the control group.

In addition to their anticancer effects on drug-tolerant breast cancer cells, repairing breast defects to enhance patient quality of life is essential [66,67]. Thus, the ability of composite scaffolds to promote breast tissue reconstruction was evaluated. Following the complete release of drugs, the composite scaffolds not only supported the adhesion and proliferation of hMSCs but also promoted the formation of lipid droplets and the expression of FASN, FABP4, CEBPA and LPL in an adipogenic environment (Figs. 6 and 7 and S21). *In vivo* tissue regeneration experiments, as shown in Fig. S23, revealed that after anticancer treatment, adjacent healthy cells migrated into the composite scaffolds. These cells underwent rapid proliferation with the support of the composite scaffolds, ultimately leading to the successful repair of breast tissue. The results highlighted the versatility of the composite scaffolds for dual purposes: (1) eradicating residual drug-tolerant breast cancer cells through synergistic magnetic hyperthermia and sensitizing chemotherapy after surgical resection and (2) facilitating breast tissue regeneration after anticancer treatment.

5. Conclusions

Multifunctional composite scaffolds (Dox-Lipo/miRNA-Lipo/Gel/PGA/FeNP) were fabricated by immobilizing Dox-encapsulated thermosensitive liposomes and miRNA-encapsulated MMP-7-cleavable liposomes in porous scaffolds of Fe_3O_4 NPs, gelatin and polyglutamic acid. The composite scaffolds had a well-interconnected porous structure and exhibited excellent magnetic-thermal conversion properties.

The composite scaffolds under AMF irradiation could increase the self-environmental temperature and accelerate Dox release from Dox-encapsulated thermosensitive liposomes in the composite scaffolds. In the presence of specific MMP-7, miRNA-encapsulated liposomes could be precisely cleaved and released from the composite scaffolds to be endocytosed by Dox-tolerant MDA-MB-231 cells. The *in vitro* and *in vivo* results showed that the composite scaffolds were able to reduce drug resistance and eliminate Dox-tolerant MDA-MB-231 cells through the synchronized synergistic effect of magnetic hyperthermia and sensitizing chemotherapy, which demonstrated more effective therapeutic potential than single treatment. Furthermore, after drug release, the composite scaffolds could support the proliferation and adipogenesis of hMSCs. The *in vivo* regeneration results demonstrated that the composite scaffolds could maintain their integrity for a long time and guide normal cell infiltration and proliferation within the scaffolds. Overall, composite scaffolds can serve as a better treatment strategy for drug-tolerant breast cancer.

CRediT authorship contribution statement

Rui Sun: Writing – review & editing, Writing – original draft, Visualization, Software, Methodology, Investigation, Formal analysis, Data curation, Conceptualization. **Man Wang:** Writing – review & editing, Writing – original draft, Investigation, Formal analysis. **Tianjiao Zeng:** Writing – review & editing, Writing – original draft, Investigation, Formal analysis. **Huajian Chen:** Writing – review & editing, Writing – original draft, Methodology, Investigation, Formal analysis. **Toru Yoshitomi:** Writing – review & editing, Writing – original draft, Methodology, Investigation, Formal analysis. **Masaki Takeguchi:** Writing – review & editing, Writing – original draft, Investigation. **Naoki Kawazoe:** Writing – review & editing, Writing – original draft, Validation, Software, Methodology, Funding acquisition, Data curation. **Yingnan Yang:** Writing – review & editing, Writing – original draft, Methodology, Conceptualization. **Guoping Chen:** Writing – review & editing, Writing – original draft, Validation, Supervision, Resources, Project administration, Methodology, Investigation, Funding acquisition, Formal analysis, Data curation, Conceptualization.

Ethics approval and consent to participate

Animal experiments were conducted with approval from the Ethical Committee of Animal Experiments of NIMS (accreditation No: 76-2023-12) and according to the Committee Guidelines.

Declaration of competing interest

Guoping Chen is an editorial board member for Bioactive Materials and was not involved in the editorial review or the decision to publish this article. All authors declare that there are no competing interests.

Acknowledgements

This research was supported by JSPS KAKENHI Grant Number 19H04475, 21H03830, 22K19926 and 24K03289.

Appendix A. Supplementary data

Supplementary data to this article can be found online at https://doi.org/10.1016/j.bioactmat.2024.10.011.

References

[1] M. MacKenzie, H. Stobart, D. Dodwell, C. Taylor, Risk of breast cancer death after a diagnosis of early invasive breast cancer, BMJ 381 (2023) 1355, https://doi.org/10.1136/bmj.p1355.

[2] A. Singh, R. Mishra, A. Mazumder, Breast cancer and its therapeutic targets: a comprehensive review, Chem. Biol. Drug Des. 103 (2024) e14384, https://doi.org/10.1111/cbdd.14384.

[3] S. McClelland, Breast cancer radiation therapy, Lancet 396 (2020) 1559, https://doi.org/10.1016/S0140-6736(20)32324-2.

[4] B. Moy, R.B. Rumble, L.A. Carey, Chemotherapy and targeted therapy for endocrine-pretreated or hormone receptor–negative metastatic breast cancer: ASCO guideline rapid recommendation update, J. Clin. Oncol. 41 (2023) 1318–1320, https://doi.org/10.1200/JCO.22.02807.

[5] M. Arnedos, C. Vicier, S. Loi, C. Lefebvre, S. Michiels, H. Bonnefoi, F. Andre, Precision medicine for metastatic breast cancer—limitations and solutions, Nat. Rev. Clin. Oncol. 12 (2015) 693–704, https://doi.org/10.1038/nrclinonc.2015.123.

[6] A.G. Waks, E.P. Winer, Breast cancer treatment: a review, JAMA 321 (2019) 288–300, https://doi.org/10.1001/jama.2018.19323.

[7] A. Bhushan, A. Gonsalves, J.U. Menon, Current state of breast cancer diagnosis, treatment, and theranostics, Pharmaceutics 13 (2021) 723, https://doi.org/10.3390/pharmaceutics13050723.

[8] Y. Wang, X. Chen, Z. Chen, X. Wang, H. Wang, H. Zhai, J. Ding, L. Yu, Autophagy inhibition mediated via an injectable and NO-releasing hydrogel for amplifying the antitumor efficacy of mild magnetic hyperthermia, Bioact. Mater. 39 (2024) 336–353, https://doi.org/10.1016/j.bioactmat.2024.05.032.

[9] W. Fan, B. Yung, P. Huang, X. Chen, Nanotechnology for multimodal synergistic cancer therapy, Chem. Rev. 117 (2017) 13566–13638, https://doi.org/10.1021/acs.chemrev.7b00258.

[10] J. Zhang, J. Li, X. Wang, N. Kawazoe, G. Chen, Targeting ligand-functionalized photothermal scaffolds for cancer cell capture and in situ ablation, Biomater. Sci. 5 (2017) 2276–2284, https://doi.org/10.1039/c7bm00639j.

[11] X. Wang, J. Li, N. Kawazoe, G. Chen, Photothermal ablation of cancer cells by albumin-modified gold nanorods and activation of dendritic cells, Materials 12 (2019) 31, https://doi.org/10.3390/ma12010031.

[12] L. Sutrisno, H. Chen, T. Yoshitomi, N. Kawazoe, Y. Yang, G. Chen, PLGA–collagen–BPNS bifunctional composite mesh for photothermal therapy of melanoma and skin tissue engineering, J. Mater. Chem. B 10 (2022) 204–213, https://doi.org/10.1039/d1tb02366g.

[13] A. Bigham, I. Fasolino, S. Borsacchi, C. Valente, L. Calucci, G. Turacchio, M. Pannico, M. Serrano-Ruiz, L. Ambrosio, M.G. Raucci, A theragenerative bio-nanocomposite consisting of black phosphorus quantum dots for bone cancer therapy and regeneration, Bioact. Mater. 35 (2024) 99–121, https://doi.org/10.1016/j.bioactmat.2024.01.018.

[14] X. Wang, J. Zhang, J. Li, Y. Chen, Y. Chen, N. Kawazoe, G. Chen, Bifunctional scaffolds for the photothermal therapy of breast tumor cells and adipose tissue regeneration, J. Mater. Chem. B 6 (2018) 7728–7736, https://doi.org/10.1039/c8tb02325e.

[15] L. Sutrisno, H. Chen, Y. Chen, T. Yoshitomi, N. Kawazoe, Y. Yang, G. Chen, Composite scaffolds of black phosphorus nanosheets and gelatin with controlled pore structures for photothermal cancer therapy and adipose tissue engineering, Biomaterials 275 (2021) 120923, https://doi.org/10.1016/j.biomaterials.2021.120923.

[16] H. Chen, X. Wang, L. Sutrisno, T. Zeng, N. Kawazoe, Y. Yang, G. Chen, Folic acid–functionalized composite scaffolds of gelatin and gold nanoparticles for photothermal ablation of breast cancer cells, Front. Bioeng. Biotechnol. 8 (2020) 589905, https://doi.org/10.3389/fbioe.2020.589905.

[17] L. Sutrisno, H. Chen, T. Yoshitomi, N. Kawazoe, Y. Yang, G. Chen, Preparation of composite scaffolds composed of gelatin and Au nanostar-deposited black phosphorus nanosheets for the photothermal ablation of cancer cells and adipogenic differentiation of stem cells, Biomater. Adv. 138 (2022) 212938, https://doi.org/10.1016/j.bioadv.2022.212938.

[18] J. Zhang, J. Li, S. Chen, N. Kawazoe, G. Chen, Preparation of gelatin/Fe 3 O 4 composite scaffolds for enhanced and repeatable cancer cell ablation, J. Mater. Chem. B 4 (2016) 5664–5672, https://doi.org/10.1039/c6tb01543c.

[19] X. Liu, J. Zheng, W. Sun, X. Zhao, Y. Li, N. Gong, Y. Wang, X. Ma, T. Zhang, L. Y. Zhao, Y. Hou, Z. Wu, Y. Du, H. Fan, J. Tian, X.J. Liang, Ferrimagnetic vortex nanoring-mediated mild magnetic hyperthermia imparts potent immunological effect for treating cancer metastasis, ACS Nano 13 (2019) 8811–8825, https://doi.org/10.1021/acsnano.9b01979.

[20] X. Liu, Y. Zhang, Y. Wang, W. Zhu, G. Li, X. Ma, Y. Zhang, S. Chen, S. Tiwari, K. Shi, S. Zhang, H.M. Fan, Y.X. Zhao, X. Liang, Comprehensive understanding of magnetic hyperthermia for improving antitumor therapeutic efficacy, Theranostics 10 (2020) 3793–3815, https://doi.org/10.7150/thno.40805.

[21] Y. Huang, J.C. Hsu, H. Koo, D.P. Cormode, Repurposing ferumoxytol: diagnostic and therapeutic applications of an FDA-approved nanoparticle, Theranostics 12 (2022) 796–816, https://doi.org/10.7150/thno.67375.

[22] H. Gavilán, S.K. Avugadda, T. Fernández-Cabada, N. Soni, M. Cassani, B.T. Mai, R. Chantrell, T. Pellegrino, Magnetic nanoparticles and clusters for magnetic hyperthermia: optimizing their heat performance and developing combinatorial therapies to tackle cancer, Chem. Soc. Rev. 50 (2021) 11614–11667, https://doi.org/10.1039/d1cs00427a.

[23] H. Zhuang, C. Qin, M. Zhang, J. Ma, D. Zhai, B. Ma, N. Ma, Z. Huan, C. Wu, 3D-printed bioceramic scaffolds with Fe_3S_4 microflowers for magnetothermal and chemodynamic therapy of bone tumor and regeneration of bone defects, Biofabrication 13 (2021) 045010, https://doi.org/10.1088/1758-5090/ac19c7.

[24] G. Wei, Y. Wang, G. Yang, Y. Wang, R. Ju, Recent progress in nanomedicine for enhanced cancer chemotherapy, Theranostics 11 (2021) 6370–6392, https://doi.org/10.7150/thno.57828.

[25] C. Wong, T. Stylianopoulos, J. Cui, J. Martin, V.P. Chauhan, W. Jiang, Z. Popović, R.K. Jain, M.G. Bawendi, D. Fukumura, Multistage nanoparticle delivery system for deep penetration into tumor tissue, Proc. Natl. Acad. Sci. U.S.A. 108 (2011) 2426–2431, https://doi.org/10.1073/pnas.1018382108.
[26] Y. Liu, Q. Yu, J. Chang, C. Wu, Nanobiomaterials: from 0D to 3D for tumor therapy and tissue regeneration, Nanoscale 11 (2019) 13678–13708, https://doi.org/10.1039/c9nr02955a.
[27] W. Ma, H. Ma, P. Qiu, H. Zhang, Z. Yang, B. Ma, J. Chang, X. Shi, C. Wu, Sprayable β-$FeSi_2$ composite hydrogel for portable skin tumor treatment and wound healing, Biomaterials 279 (2021) 121225, https://doi.org/10.1016/j.biomaterials.2021.121225.
[28] Y. Zheng, J. Wu, Y. Zhu, C. Wu, Inorganic-based biomaterials for rapid hemostasis and wound healing, Chem. Sci. 14 (2023) 29–53, https://doi.org/10.1039/d2sc04962g.
[29] R. Sun, H. Chen, M. Wang, T. Yoshitomi, M. Takeuchi, N. Kawazoe, Y. Yang, G. Chen, Smart composite scaffold to synchronize magnetic hyperthermia and chemotherapy for efficient breast cancer therapy, Biomaterials 307 (2024) 122511, https://doi.org/10.1016/j.biomaterials.2024.122511.
[30] R. Sun, H. Chen, L. Sutrisno, N. Kawazoe, G. Chen, Nanomaterials and their composite scaffolds for photothermal therapy and tissue engineering applications [J]. Science and technology of advanced materials, Sci. Technol. Adv. Mater. 22 (2021) 404–428, https://doi.org/10.1080/14686996.2021.1924044.
[31] Z. Zhang, C. He, X. Chen, Designing hydrogels for immunomodulation in cancer therapy and regenerative medicine, Adv. Mater. 36 (2024) e2308894, https://doi.org/10.1002/adma.202308894.
[32] B. Colak, Y.N. Ertas, Implantable, 3D-printed alginate scaffolds with bismuth sulfide nanoparticles for the treatment of local breast cancer via enhanced radiotherapy, ACS Appl. Mater. Interfaces 16 (2024) 15718–15729, https://doi.org/10.1021/acsami.3c17024.
[33] L. Yu, F. Sun, Y. Wang, W. Li, Y. Zheng, G. Shen, Y. Wang, M. Chen, Effects of MgO nanoparticle addition on the mechanical properties, degradation properties, antibacterial properties and in vitro and in vivo biological properties of 3D-printed Zn scaffolds, Bioact. Mater. 37 (2024) 72–85, https://doi.org/10.1016/j.bioactmat.2024.03.016.
[34] Q. Li, A. Wang, J. Li, S. Liang, Y. Tian, S. Bai, A synergistic therapy strategy for hypoxic solid tumor therapy, Matter 5 (2022) 2425–2428, https://doi.org/10.1016/j.matt.2022.05.017.
[35] H. Sun, Q. Zhang, J. Li, S. Peng, X. Wang, R. Cai, Near-infrared photoactivated nanomedicines for photothermal synergistic cancer therapy, Nano Today 37 (2021) 101073, https://doi.org/10.1016/j.nantod.2020.101073.
[36] J. Zhu, Y. Zhang, Z. Li, X. Bao, Y. Zhou, B. Ma, Y. Xie, P. Yan, Z. Wu, Q. Zhang, J. Zou, X. Chen, Tumor-microenvironment-responsive poly-prodrug encapsulated semiconducting polymer nanosystem for phototherapy-boosted chemotherapy, Mater. Horiz. 10 (2023) 3014–3023, https://doi.org/10.1039/d3mh00242j.
[37] W. Pan, C. Liu, Y. Li, Y. Yang, W. Li, C. Feng, L. Li, Ultrathin tellurium nanosheets for simultaneous cancer thermo-chemotherapy, Bioact. Mater. 13 (2021) 96–104, https://doi.org/10.1016/j.bioactmat.2021.11.010.
[38] Y. Wang, D. Pattarayan, H. Huang, Y. Zhao, S. Li, Y. Wang, M. Zhang, S. Li, D. Yang, Systematic investigation of chemo-immunotherapy synergism to shift anti-PD-1 resistance in cancer, Nat. Commun. 15 (2024) 3178, https://doi.org/10.1038/s41467-024-47433-y.
[39] S. Mura, J. Nicolas, P. Couvreur, Stimuli-responsive nanocarriers for drug delivery, Nat. Mater. 12 (2013) 991–1003, https://doi.org/10.1038/nmat3776.
[40] H. Liu, T. Prachyathipsakul, T.M. Koyasseril-Yehiya, S.P. Le, S. Thayumanavan, Molecular bases for temperature sensitivity in supramolecular assemblies and their applications as thermoresponsive soft materials, Mater. Horiz. 9 (2022) 164–193, https://doi.org/10.1039/d1mh01091c.
[41] J.Q. Wang, Y. Yang, C.Y. Cai, Q.X. Teng, Q. Cui, J. Lin, Y.G. Assaraf, Z.S. Chen, Multidrug resistance proteins (MRPs): structure, function and the overcoming of cancer multidrug resistance, Drug Resist. Updat. 54 (2021) 100743, https://doi.org/10.1016/j.drup.2021.100743.
[42] S. Liu, A.R. Khan, X. Yang, B. Dong, J. Ji, G. Zhai, The reversal of chemotherapy-induced multidrug resistance by nanomedicine for cancer therapy, J. Contr. Release 335 (2021) 1–20, https://doi.org/10.1016/j.jconrel.2021.05.012.
[43] W. Zhang, Y. Chen, M. Li, S. Cao, N. Wang, Y. Zhang, Y. Wang, A PDA-functionalized 3D lung scaffold bioplatform to construct complicated breast tumor microenvironment for anticancer drug screening and immunotherapy, Adv. Sci. 10 (2023) 2302855, https://doi.org/10.1002/advs.202302855.
[44] Y. Peng, X. Zhu, L. Qiu, Electroneutral composite polymersomes self-assembled by amphiphilic polyphosphazenes for effective miR-200c in vivo delivery to inhibit drug resistant lung cancer, Biomaterials 106 (2016) 1–12, https://doi.org/10.1016/j.biomaterials.2016.08.001.
[45] V. Juang, C.H. Chang, C.S. Wang, H.E. Wang, Y.L. Lo, pH-responsive PEG-shedding and Targeting peptide-modified nanoparticles for dual-delivery of Irinotecan and microRNA to enhance tumor-specific therapy, Small 15 (2019) 1903296, https://doi.org/10.1002/smll.201903296.
[46] S. Safaei, M. Amini, S. Najjary, A. Mokhtarzadeh, N. Bolandi, H. Saeedi, N. Alizadeh, D. Javadrashid, B. Baradaran, miR-200c increases the sensitivity of breast cancer cells to Doxorubicin through downregulating MDR1 gene, Exp. Mol. Pathol. 125 (2022) 104753, https://doi.org/10.1016/j.yexmp.2022.104753.
[47] N.E. Sounni, A. Noel, Targeting the tumor microenvironment for cancer therapy, Clin. Chem. 59 (2013) 85–93, https://doi.org/10.1373/clinchem.2012.185363.
[48] S. Thakkar, D. Sharma, K. Kalia, R.K. Tekade, Tumor microenvironment targeted nanotherapeutics for cancer therapy and diagnosis: a review, Acta Biomater. 101 (2020) 43–68, https://doi.org/10.1016/j.actbio.2019.09.009.
[49] M. Shahriari, M. Zahiri, K. Abnous, S.M. Taghdisi, M. Ramezani, M. Alibolandi, Enzyme responsive drug delivery systems in cancer treatment, J. Contr. Release 308 (2019) 172–189, https://doi.org/10.1016/j.jconrel.2019.07.004.
[50] J. Yang, Y. Yang, N. Kawazoe, G. Chen, Encapsulation of individual living cells with enzyme responsive polymer nanoshell, Biomaterials 197 (2019) 317–326, https://doi.org/10.1016/j.biomaterials.2019.01.029.
[51] A. Tanaka, Y. Fukuoka, Y. Morimoto, T. Honjo, D. Koda, M. Goto, T. Maruyama, Cancer cell death induced by the intracellular self-assembly of an enzyme-responsive supramolecular gelator, J. Am. Chem. Soc. 137 (2015) 770–775, https://doi.org/10.1021/ja510156v.
[52] G. Nagel, A. Sousa-Herves, S. Wedepohl, M. Calderón, Matrix metalloproteinase-sensitive multistage nanogels promote drug transport in 3D tumor model, Theranostics 10 (2020) 91–108, https://doi.org/10.7150/thno.34851.
[53] O. Kousidou, A. Roussidis, A. Theocharis, N. Karamanos, Expression of MMPs and TIMPs genes in human breast cancer epithelial cells depends on cell culture conditions and is associated with their invasive potential, Anticancer Res. 24 (2004) 4025–4030.
[54] R. Sun, H. Chen, J. Zheng, T. Yoshitomi, N. Kawazoe, Y. Yang, G. Chen, Composite scaffolds of gelatin and Fe3O4 nanoparticles for magnetic hyperthermia-based breast cancer treatment and adipose tissue regeneration, Adv. Healthcare Mater. 12 (2023) 2202604, https://doi.org/10.1002/adhm.202202604.
[55] K. Zhang, L. Song, J. Wang, S. Yan, G. Li, L. Cui, J. Yin, Strategy for constructing vascularized adipose units in poly (l-glutamic acid) hydrogel porous scaffold through inducing in-situ formation of ASCs spheroids, Acta Biomater. 51 (2017) 246–257, https://doi.org/10.1016/j.actbio.2017.01.043.
[56] H. Chen, R. Sun, J. Zheng, N. Kawazoe, Y. Yang, G. Chen, Doxorubicin-encapsulated thermosensitive liposome-functionalized photothermal composite scaffolds for synergistic photothermal therapy and chemotherapy, J. Mater. Chem. B 10 (2022) 4771–4782, https://doi.org/10.1039/d2tb00993e.
[57] K.J. Isaacson, M.M. Jensen, N.B. Subrahmanyam, H. Ghandehari, Matrix-metalloproteinases as targets for controlled delivery in cancer: an analysis of upregulation and expression, J. Contr. Release 259 (2017) 62–75, https://doi.org/10.1016/j.jconrel.2017.01.034.
[58] B.R. Rushing, S. Molina, S. Sumner, Metabolomics analysis reveals altered metabolic pathways and response to doxorubicin in drug-resistant triple-negative breast cancer cells, Metabolites 13 (2023) 865, https://doi.org/10.3390/metabo13070865.
[59] L. Bao, S. Hazari, S. Mehra, D. Kaushal, K. Moroz, S. Dash, Increased expression of P-glycoprotein and doxorubicin chemoresistance of metastatic breast cancer is regulated by miR-298, Am. J. Pathol. 180 (2012) 2490–2503, https://doi.org/10.1016/j.ajpath.2012.02.024.
[60] M. Świętek, A. Brož, J. Tarasiuk, S. Wroński, W. Tokarz, A. Kozieł, M. Błażewicz, L. Bačáková, Carbon nanotube/iron oxide hybrid particles and their PCL-based 3D composites for potential bone regeneration, Mater. Sci. Eng. C. 104 (2019) 109913, https://doi.org/10.1016/j.msec.2019.109913.
[61] D.H. Manicourt, N. Fujimoto, K. Obata, E.J.M.A. Thonar, Serum levels of collagenase, stromelysin-1, and timp-1, Arthritis Rheum. 37 (1994) 1774–1783, https://doi.org/10.1002/art.1780371211.
[62] Y. Qi, H. Min, A. Mujeeb, Y. Zhang, X. Han, X. Zhao, G. Anderson, Y. Zhao, G. Nie, Injectable hexapeptide hydrogel for localized chemotherapy prevents breast cancer recurrence, ACS Appl. Mater. Interfaces 10 (2018) 6972–6981.
[63] W. Gao, Y. Zheng, R. Wang, H. Chen, X. Cai, G. Lu, L. Chu, C. Xu, N. Zhang, Z. Wang, H. Ran, P. Li, C. Yang, Z. Mei, J. Song, A smart, phase transitional and injectable DOX/PLGA-Fe implant for magnetic-hyperthermia-induced synergistic tumor eradication, Acta Biomater. 29 (2016) 298–306.
[64] Y. Zheng, Y. Yan, L. Lin, Q. He, H. Hu, R. Luo, D. Xian, J. Wu, Y. Shi, F. Zeng, C. Wu, G. Quan, C. Lu, Titanium carbide MXene-based hybrid hydrogel for chemo-photothermal combinational treatment of localized bacterial infection, Acta Biomater. 142 (2022) 113–123, https://doi.org/10.1016/j.actbio.2022.02.019.
[65] F. Gao, W. Xie, Y. Miao, D. Wang, Z. Guo, A. Ghosal, Y. Li, Y. Wei, S.S. Feng, L. Zhao, H.M. Fan, Magnetic hydrogel with optimally adaptive functions for breast cancer recurrence prevention, Adv. Healthcare Mater. 8 (2019) 1900203, https://doi.org/10.1002/adhm.201900203.
[66] G. Bai, P. Yuan, B. Cai, X. Qiu, R. Jin, S. Liu, Y. Li, X. Chen, Stimuli-responsive scaffold for breast cancer treatment combining accurate photothermal therapy and adipose tissue regeneration, Adv. Funct. Mater. 29 (2019) 1904401, https://doi.org/10.1002/adfm.201904401.
[67] B. Chen, H. Xiang, S. Pan, L. Yu, T. Xu, Y. Chen, Advanced theragenerative biomaterials with therapeutic and regeneration multifunctionality, Adv. Funct. Mater. 30 (2020) 2002621, https://doi.org/10.1002/adfm.202002621.